Check for updates

Energy Technology
Generation, Conversion, Storage, Distribution
www.entechnol.de

Technical Aspects of Natural Gas Pyrolysis in Liquid Metal Bubble Column Reactors

Christoph Hofberger, Benjamin Dietrich, Ralf Krumholz, Adam Paul Noglik, Michael Olbricht, Sabine Schatzmann, Leonid Stoppel, Marie Richter, Neele Uhlenbruck, and Thomas Wetzel*

The pyrolysis of low alkanes (in the following short "pyrolysis") has already been investigated during the 1960s. However, none of the reactor systems used at the time are capable of continuous operation. Therefore, the Karlsruhe Institute of Technology has intensified the development of the promising liquid metal bubble column technology in recent years, which is capable of continuous operation. Various key aspects have been addressed, such as scale-up and the pyrolysis of high-caloric natural gas. Herein, further developments for a pilot scale system have been investigated, which concern increased throughput and long-term operation capabilities. Careful evaluation of the impact of according measures has been done, which shows that the achieved scale-up has only negligible effects on the pyrolysis outcome. The effects of the scale-up on residence times are negligible. The bubble formation behavior depends on the throughput and the characteristics of the orifice. Wall effects are marginal. Fundamental minimization of weeping could not be confirmed. Reactor pre-chambers in combination with tin collection chambers are recommended for further scale-up. An increase in the volume flow should be examined. In terms of long-term operation , head as well as feed pressure control is recommended.

1. Introduction

The pyrolysis of hydrocarbons is a research topic that was extensively studied for the past decades.[1–3] While first investigations were related to pyrolysis in general and carried out primarily in tubular reactors, in the 60s of the 20th century, the research on pyrolysis was intensified and specific branches developed, among them methane pyrolysis. The studies published recently concern not only gaseous hydrocarbon pyrolysis[4,5] but also biogas,[6,7] biomass,[8–10] and plastic waste[11,12] pyrolysis. The currently published hydrocarbon pyrolysis-related publications concern catalysis[13–15] and the utilization of the carbon by-products.[16] Patlolla et al.[4] summarized reactor types existing for methane pyrolysis (**Figure 1**).

In a review by Khan et al.[17] in 1970, most of the pyrolysis studies focused on methane pyrolysis in different tube reactors and shock wave reactors. Khan et al.[17] concluded that pure methane (PM) pyrolysis is a first-order radical chain reaction. They also found that the inner surface conditions of the reactors seem to have an influence on the pyrolysis results. Investigations of hydrogen inhibition,[17] however, produced contradictory results which probably occurred due to different temperature ranges (hydrogen inhibition between 1373 and 2473 K; no hydrogen inhibition between 1656 and 1965 K), different reactor types (tubular and annular reactors), reactor materials (graphite, porcelain, and quartz), or reactor operation modes (shock-tube and non-shock-tube). The reactors used in these studies were not suitable for continuous operation. In tubular and annular reactors, for example, carbon deposits were formed on the hot inner surfaces of the reactor, which changed the reactor geometries (e.g., reactor diameter and residence time) or the thermodynamics (e.g., catalyst surface and heat transfer). Ultimately, the carbon deposition can lead to complete clogging. To overcome this challenge, methane was diluted with nitrogen, argon, or hydrogen in some studies.[18–24] Nitrogen or hydrogen dilution of the feed leads to a reduction of carbon deposits, but probably affects the pyrolysis reaction and product composition[25,26] as well.

Technologies, such as fluid wall reactors, avoid the dilution of the feed.[4] On the other hand, the product gas is diluted by the

C. Hofberger, B. Dietrich, R. Krumholz, L. Stoppel, M. Richter, N. Uhlenbruck, T. Wetzel
Karlsruhe Liquid Metal Laboratory
Karlsruhe Institute of Technology
76133 Eggenstein-Leopoldshafen, Baden-Württemberg, Germany
E-mail: christoph.hofberger@kit.edu

A. P. Noglik, M. Olbricht, S. Schatzmann
Wintershall Dea AG
29221 Kassel, Hessen, Germany

M. Olbricht
Faculty of Mechanical Engineering
Technical University of Applied Sciences Würzburg-Schweinfurt
97421 Schweinfurt, Germany

The ORCID identification number(s) for the author(s) of this article can be found under https://doi.org/10.1002/ente.202400183.

© 2024 The Author(s). Energy Technology published by Wiley-VCH GmbH. This is an open access article under the terms of the Creative Commons Attribution-NonCommercial-NoDerivs License, which permits use and distribution in any medium, provided the original work is properly cited, the use is non-commercial and no modifications or adaptations are made.

DOI: 10.1002/ente.202400183

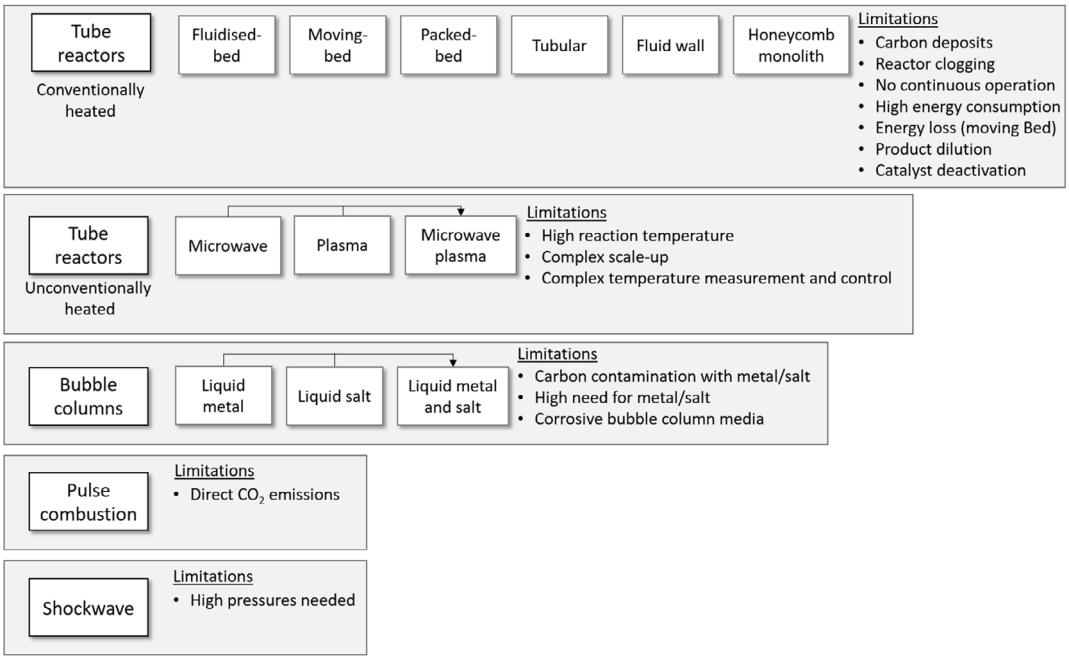

Figure 1. List of common pyrolysis reactor designs and their characteristics.[4]

wall gas anyway, which leads to a higher product volume flow and thus enhancing heat removal from the reactor. And even if the feed is not diluted, dilution effects can occur over the reactor length. Shock-tube and non-shock-tube reactors cannot be operated continuously. They are used for studies of reaction mechanisms. Other reactor types, such as fluidized-bed reactors[27] and plasma reactors,[28] can be operated continuously and inhibit clogging. However, both reactor types are associated with several challenges. The heat transfer from the heating system to the bed material needs to be improved, for example. When using catalytic material for the floating bed, the necessary temperature can be lowered, but the catalyst is inactivated by the carbon adhering to the bed material, which has to be replaced or reactivated. When using carbon black as bed material, no separation is required. On the other hand, according to some researchers, carbon materials can have only small catalytic effects.[4] Anyway, additional to the carbon, the bed material has to be removed constantly from the reactor, which leads to increased heat removal depending on the heat capacity of the bed material. Nevertheless, moving bed reactors are constantly developed toward industrial applications, for example, by BASF.[29–31] Fluidized bed reactors are in development as well. These reactors were developed, for example, by the Hazer Group and the Florida Solar Energy Centre.[29,32,33]

Plasma reactors are mostly designed to produce high-quality carbon,[4] but show low efficiency[34] and an product gas stream, which is enriched with C_2H_x hydrocarbons.[35,36] Microwave and combined microwave-plasma reactors require lower temperatures due to the microwave mechanisms, but lab scale experiments reveal difficulties such as hot spots and are challenging to scale up.[4] Therefore also for the plasma technology, some projects are ongoing, presently. Monolith materials,[37] for example, built a production plant (Olive Creek Plant), which is optimized for the production of carbon black. The Tomsk Universities and TOMSK-GAZPROM[38,39] developed a combined microwave-plasma torch catalyst bed reactor.[29]

Another technology to prevent carbon clogging is the use of high-temperature liquids such as liquid metals (LM) or liquid salts for bubble columns or plug and mist reactors. Molten metal plug and mist reactors[4,40] maximize the contact surface area between the metal and the gas, so they need a lower amount of metal compared to bubble column reactors. On the other hand, it is necessary to pump liquid metal, which is not trivial at high temperatures. Bubble columns in turn use stagnant high-temperature fluids. Both LM and liquid salts can be used as liquid phase. Both fluid types are capable for concentrated solar power (CSP) plants.[41–43] For LM, in particular liquid tin, a direct CSP heated bubble column reactor has already been tested successfully by Msheik et al.[44]

Liquid salts, however, have several disadvantages, compared to LM: A lower thermal conductivity[45] and low catalytic activities.[4,46] In addition, salts are limited in their usable temperature range.[45,47] In general, the melting temperature of salt is high compared to LM,[47] and in some cases, the decomposition of salts begins at 800 K.[10] The use of LM on the other hand is only limited due to their vapor pressure, respectively, their melting and boiling temperature. This temperature range is usually wider than the usable temperature range of liquid salts.[47] Additionally, LMs can be easily combined with catalytic additives (examples are shown in **Table 1**), as metals were assumed to have the highest potential as pyrolysis catalysts.[4,48]

In this study, effects were investigated, which are of interest for long-term operation and for a scale-up. Therefore, catalytically active metals or alloys were not used. Only the general characteristics of LM as the high thermal conductivity and density were utilized. Due to the high difference in density between liquid tin and carbon, for example, the produced carbon accumulates

© 2024 The Author(s). Energy Technology published by Wiley-VCH GmbH

21944296, 0, Downloaded from https://onlinelibrary.wiley.com/doi/10.1002/ente.202400183 by Christoph Hofberger , Wiley Online Library on [16/07/2024]. See the Terms and Conditions (https://onlinelibrary.wiley.com/terms-and-conditions) on Wiley Online Library for rules of use; OA articles are governed by the applicable Creative Commons License

Table 1. Examples for catalytic metals and alloys for the pyrolysis in liquid metal bubble columns.

Metals	Outcome	Publications
Ni-Bi	High catalytic activity of Ni–Bi alloys, in particular 27% Ni and 73% Bi	[14,48,93]
Te	High catalytic activity of pure Te and moderate activity of Ta–Ni alloys	[15]
Ga	Catalytic activity of Ga needs further validation	[94]
Ni-Sn	Catalytic activity of Ni–Sn alloys, in particular 5% Ni an 95% Sn	[95,96]

Table 2. Melting and boiling points and safety information of metals with a melting point below 1223 K and a boiling point above 1473 K. Radioactive metals are excluded.

Metal	Melting point [K]	Boiling point [K]	Safety information[a)]	Literature
Al	933	2715	Limited flammable	[97,98]
Ca	1115	1760	Limited flammable	[97,98]
Ga	303	2673	Harmful	[97,98]
Ge	1211	3103	Limited flammable	[97,98]
In	430	2273	Limited flammable	[97,99]
Sn	505	2893	–	[97,98]
Sb	904	1908	Toxic	[97,98]
La	1193	3743	Flammable	[97,98]
Ce	1068	3743	Limited flammable	[97,98]
Pr	1208	3403	Limited flammable	[97,98]
Eu	1099	1986	Limited flammable	[97,98]
Yb	1097	1703	Limited flammable, moderately toxic	[97,98]
Pb	600	2017	Hazardous, environmental hazard	[97,98]

[a)]GESTIS Substance Database—10.04.2024.

as loose bulk, floating on the liquid tin[49] and does not lead to clogging of the reactor. The melting point of the used metal should be below 1223 K and boiling point above 1473 K, as these are the aimed reaction temperatures. To keep the loss of metal due to the vapor pressure as small as possible, boiling points greatly above 1473 K are advantageous. The list of metals that are liquids within these temperatures contains 13 (nonradioactive) metals (**Table 2**).

Tin is the only metal in this range, which is not afflicted by any safety issues. It shows a broad temperature range of liquid state, and the boiling point is far from the maximum pyrolysis temperature of this study (max. 1473 K).

One of the first reports of methane pyrolysis in a bubble column was published by Kaffes,[50] who carried out a steam reforming process in a sodium phosphate melt with nickel as catalyst. Based on the pyrolysis experiments of Abánades et al.[51] in 2012 and the present advantages and its vast expertise in the area of LM, the KIT decided in favor of the combination of bubble columns and pyrolysis reaction to develop the liquid metal bubble column technology[49,51–53] (**Table 3**).

Table 3. Overview of publication, concerning the development of the pyrolysis technology at the KIT, originating from the pyrolysis experiments of Abánades et al.[51]

Lead author	Pub.	Outcome
Plevan	[49]	• Proof-of-concept of the reactor design for methane pyrolysis in a bubble column (stainless steel) • Methane conversion dependencies (temperature, dilution, flow rate, residence time, tube material, and porosity) • Reactor material lifetime
Geißler	[52]	• Proof-of-concept of the reactor design for methane pyrolysis in a bubble column (quartz glass) • Methane conversion dependencies (temperature, tin filling level, flow rate)
Abánades	[53]	• Socio-economic analysis • Environmental impact • Scalability • Technical feasibility
Geißler	[58]	• Methane conversion dependencies (temperature, flow rate, and packed bed) • Carbon powder characterization
Uhlenbruck	[72]	• Model development for soot formation • Good agreement of model results and experimental data
Hofberger	[56]	• Scale-Up • Development of evaluation methodology for following experiments
Hofberger	[57]	• Feasibility of MEM pyrolysis • Feasibility of nGH pyrolysis • Impact of feed gas admixtures

The advantages of this technology already become obvious in the early studies by Plevan et al.[49] no clogging is formed due to formed carbon, high possible pyrolysis temperatures, and accumulation of carbon as a loose powder on the tin surface. In addition, the tin used as bubble column fluid has a low vapor pressure, which leads to low tin losses due to the discharge of tin vapor via the product gas stream. The admixture of catalytically active metals is conceivable as well.[54,55] The catalytic activities are higher than those of salt or other nonmetallic catalysts.[4] Hofberger et al.[56,57] also succeeded in scaling up the reactor system by factor 3.75 and in pyrolyzing different gas admixtures to PM as well as commercial nGH. The results of pyrolysis in an enlarged reactor and of nGH pyrolysis were then compared to those of Geißlers et al.[52,58,59] The scale-up had no significant effects on methane conversion.[56] nGH pyrolysis, on the other hand, significantly increases methane conversion in the lower (≈1223 K) and middle (≈1323 K) temperature ranges, due to the lower activation energy and enthalpy of ethane pyrolysis. The formation of H- and CH_3-radicals at lower temperatures accelerates subsequently the methane pyrolysis.[57] Hofberger et al.[57] compared these results on the basis of the analyzed product gas compositions. The pyrolysis of higher hydrocarbons should continue the effects, seen at methane–ethane–mixture (MEM) pyrolysis.[60–62]

Apart from the feed gas variations, the system was subject to a consequent alteration in view of aspects, relevant for later scale-up to pilot scale, starting from the design proposed by

© 2024 The Author(s). Energy Technology published by Wiley-VCH GmbH

21944296, 0, Downloaded from https://onlinelibrary.wiley.com/doi/10.1002/ente.202400183 by Christoph Hofberger , Wiley Online Library on [16/07/2024]. See the Terms and Conditions (https://onlinelibrary.wiley.com/terms-and-conditions) on Wiley Online Library for rules of use; OA articles are governed by the applicable Creative Commons License

Geißler et al.[52,58,59] The reactors studied differed in geometry and peripheral equipment, but all were designed for temporary use.

The aim of this study is to increase the throughput and the life time of the reactor system, without interfering the fluid mechanical characteristics of the system such as bubble formation and bubble rise behavior. Life time limiting processes concern essentially unintended carbon and tin deposits. To achieve these objectives, several changes of the system and reactor design were investigated about their impact on throughput and continuous operation. As the reactor geometry can have an elementary influence on fluid dynamics,[63] these differences were characterized and discussed in detail. In order to estimate the influence of changes of the considered system components on the fluid mechanics and thus possibly on the pyrolysis product, correlations were identified to characterize their impact on fluid dynamics. Commencing with the description of the general reactor design, several process units of the reactor were successively inspected. Besides the general reactor design aspects, the temperature is one of the most basic conditions for chemical reactions.[56] Therefore, the temperature distribution and management as soon as influences on it were discussed first. Subsequently, the reactor geometry variations were rasterized in general, followed by the orifice geometrics. These characteristics were discussed about their influence on the bubble behavior and so the residence time. As mentioned earlier, tin deposits, in particular in the reactor inlet, lowered the life time of the system in recent studies. Hence, prechambers were compared to direct gas supply of the orifice concerning bubble formation and weeping. Weeping is defined as the fluid mass flow in bubble columns through the orifice or nozzle in the opposite direction to the gas volume flow.[64] As the second identified life time-limiting process was carbon accumulation, the carbon management was discussed as well. Finally, based on a detailed comparison of the experimental set-ups and their characteristics and impacts on the pyrolysis operation, recommendations are derived for the development of a pilot-scale system.

2. Design Aspects

2.1. General Design Aspects

The actual core of the system is the liquid metal system, containing the subject of investigation: The liquid metal bubble column reactor (LMBCR) embedded in an electrically heated column furnace is shown in **Figure 2**.

The basic construction of the LMBCR is based on a quartz glass pipe, closed on one side. Quartz glass is used due to the high corrosiveness of liquid tin for iron- and nickel-based materials.[65–68] The closed side contains a dispersion unit, such as an orifice, and a reactor inlet pipe. Optionally, a reactor prechamber was inserted between the dispersion unit and the inlet pipe (Figure 2). In this study, prechambers were investigated due to their effects on fluid dynamics. Packed bed materials were not used in any of the experiments. The reactor mounting and length was designed to keep the prechamber outside of the reactor and either heating zones. Additionally, if implemented, the prechamber was cooled actively to prevent pyrolysis. On the inlet pipe side

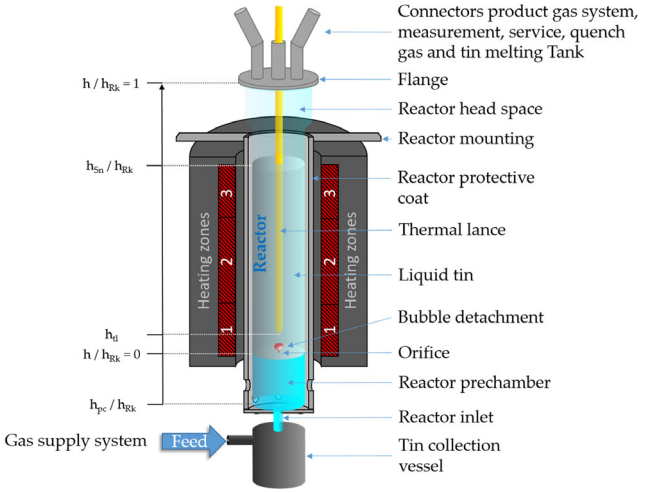

Figure 2. Schematic illustration of the reactor in a three-heating-zones furnace (not in scale).

of the reactor, the feed gas was delivered by the gas supply system. A tin collecting vessel (Section 2.7) can be inserted between inlet pipe and gas supply. In this study, six reactor designs have been examined (**Table 4**).

For experiments utilizing reactor type (RT) IV and V, the tin used consisted partly of recovered tin from previous experiments (Table 4: recycled tin amount). Although the same bubble column design was used for RT V and VI, these two reactor types differed by periphery. Besides the absence of a tin collection vessel and the usage of an unused charge of tin, RT VI the reactor prechamber was equipped with additional thermocouples. In general, all variations in reactor design were amid to identify design aspects, which are advantageous for increased throughput and long-term operability.

Due to the exothermic character of the pyrolysis reaction,[2] heat measurement and control play an important role.

2.2. Temperature Management

The tin temperature is measured at several vertical positions inside the LMBCR. To protect the thermocouples (0.5 mm Type K, VXS coated thermocouples) from the highly corrosive liquid tin, they are embedded in an Al_2O_3 tube that is closed on one side, with an outer diameter of 6 mm and an inner diameter of 4 mm. Al_2O_3 has a high chemical stability in direct contact with liquid tin.[67]

After inserting the thermocouples, the tube is closed on the open side, using a committal gas tight epoxy adhesive (JB weld). The thermocouples are then protected against the corrosive tin and oxygen. Additionally, convection streams are prevented from leaving the thermocouple lance (TCL). This TCL installed in the reactor center, as shown in Figure 2, provides height-dependent temperatures of the liquid tin and the reactor head gas volume. An example of the measured distribution is given in **Figure 3** for several reactor types and superficial gas velocities (SGVs).

Due to the different inner diameters and volume flows in RT I with an SGV of 2.5 mm s^{-1} and in RT II with an SGV

© 2024 The Author(s). Energy Technology published by Wiley-VCH GmbH

21944296, 0, Downloaded from https://onlinelibrary.wiley.com/doi/10.1002/ente.202400183 by Christoph Hofberger , Wiley Online Library on [16/07/2024]. See the Terms and Conditions (https://onlinelibrary.wiley.com/terms-and-conditions) on Wiley Online Library for rules of use; OA articles are governed by the applicable Creative Commons License

Table 4. Summary of all used reactor types including their specifications.

Reactor Type (RT)	Reactor outer diameter [mm]	Inlet system	Orifice	Recycled tin amount	Carbon discharge
I	45[59]	–	Single hole	–	–
II	80	Prechamber	Single hole	–	–
III	80	Prechamber; tin collection vessel	Single hole	–	–
IV	80	Tin collection vessel	Single hole	74–85%	–
V	80	Prechamber; tin collection vessel	Triple hole	79–100%	Yes
VI	80	Prechamber	Triple hole	–	Yes

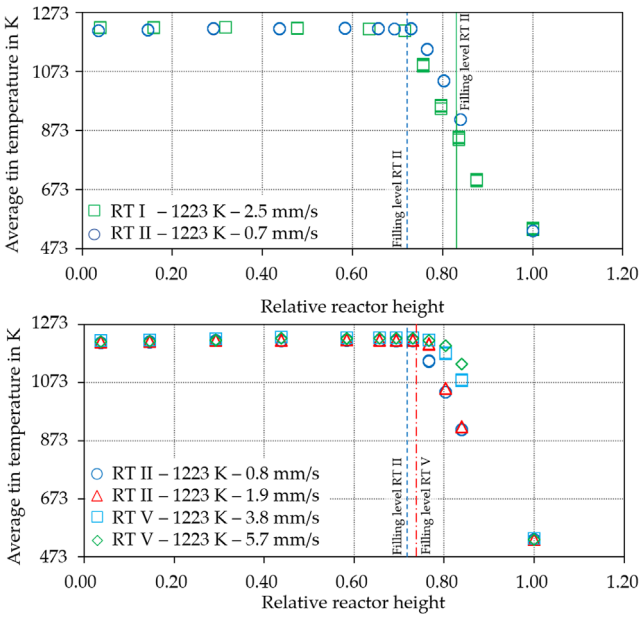

Figure 3. Comparison of temperature distributions over the relative height (h/h_{Rk}) of reactor types (RT) I and II at similar volume flows and comparison of temperature distributions at several volume flows in RT II and RT V. Uncertainty of measurements accordance with the Guide to the Expression of Uncertainty in Measurement (GUM[92]) for relative reactor height: $\leq\pm0.01$ and for average tin temperature: $\leq\pm15$ K.

of 0.7 mm s^{-1} are similar. The relative liquid tin filling levels at 1223 K are 0.83 (h_{Sn}/h_{Rk}) for RT I, 0.72 (h_{Sn}/h_{Rk}) for RT II and 0.74 (h_{Sn}/h_{Rk}) for RT V. In general, the tin temperature distribution shows only negligible fluctuations over time for each point (standard deviation $<\pm5$ K), and the thermocouples are specified to have an accuracy of $\pm \leq (T \times 0.0075)$. Above the liquid tin, the temperature decreases rapidly. These trends are observed for all tin temperatures and LMBCR designs examined. Prechambers show no measurable effects on this temperature distribution within the liquid tin. As seen in the comparison of RT II at 1223 K between 0.8 and 1.9 mm s^{-1}, the difference in SGV seems to cause no significant difference between the temperature gradients. In RT V at 1223 K between 3.8 and 5.7 mm s^{-1}, the gradients differ from each other. Higher SGVs (or volume flows) lead to higher temperatures in the reactor head space. The reactor head space is defined as the reactor volume above the liquid tin, as schematically illustrated in Figure 2. This could be observed for every tin temperature: Only with clearly increased SGVs, the head space temperatures increased slightly. Data from different LMBCR types are difficult to compare. The reactor head space temperature is strongly dependent on its insulation (as well as on cooling and heating), which is why comparability cannot be ensured. On the other hand, the reactor head flange is consistently heated to 533 K to prevent adhesion of solidified tin on the head space and flange in all experiments. At high SGVs, active cooling of the reactor head and head flange is required to keep the head flange temperature consistently below 573 K to prevent damages to the head flange sealing.

The reactor inlet is equipped with a 0.5 mm thermocouple as well. For LMBCRs with and without a reactor prechamber, this thermocouple is placed 10 mm below the orifice (**Figure 4**).

A reproducible temperature difference between reactors with and without prechamber could not be determined using this thermocouple. The inlet nozzle can be both cooled and heated actively, whereas the LMBCR prechamber is cooled consistently to prevent pyrolysis. Precise temperature management in the LMBCRs is a critical factor for reaction control. Seamless integration reaction control with reactor geometry optimization will result in significant improvements.

2.3. Reactor Geometry

As mentioned earlier, the LMBCR was scaled up by a factor of 3.75 (in terms of volume) in recent studies by Hofberger et al.[56] compared to earlier generations described by Geißler et al.[52,58,59] The LMBCR height and the tin filling level were kept approximately constant, while the diameter was increased. Developing from RT I to RT II, the inner diameter was increased by the factor of 1.84. Afterward, the increased inner diameter was left constant for all other RTs, so the reactor height to inner diameter ratio was approximately the same for RT II to RT VI (**Table 5**). In doing so, the influence of the diameter of the reactor on the product gas composition[56] could be investigated. One aim of increasing the LMBCR diameter was to subsequently install multihole dispersion units. A minimal distance of the holes of a multihole orifice is required to minimize coalescence during bubble formation,[69,70] which would lead to high bubble volumes. Depending on the inner bubble column diameter in relation to the bubble diameter, wall effects can occur and affect the bubble rise velocity.[63] The bubble rise velocity in turn defines the residence time of the gas bubbles in the hot liquid tin[56] and, thus, has an influence on the heat transfer.

© 2024 The Author(s). Energy Technology published by Wiley-VCH GmbH

21944296, 0, Downloaded from https://onlinelibrary.wiley.com/doi/10.1002/ente.202400183 by Christoph Hofberger , Wiley Online Library on [16/07/2024]. See the Terms and Conditions (https://onlinelibrary.wiley.com/terms-and-conditions) on Wiley Online Library for rules of use; OA articles are governed by the applicable Creative Commons License

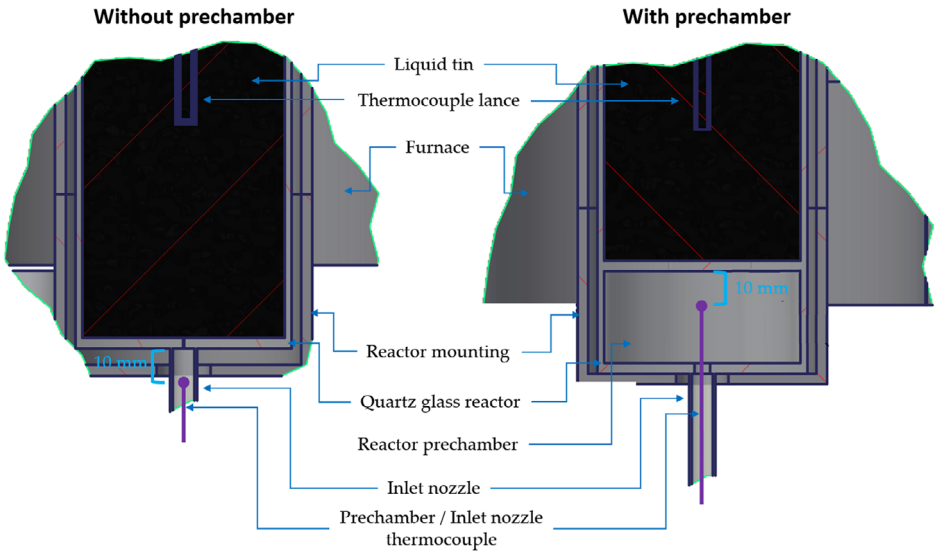

Figure 4. Bottom of a reactor without a reactor prechamber (left) and with reactor prechamber (right) with the thermocouple position.

Table 5. Ratios of the approx. Constant reactor heights (h_{Rk})[a)] to the upscaled parameter of inner diameter (d_{Rk}) and ß values of this study.

Reactor type	$\frac{h_{Rk}}{d_{Rk,i}}$	$ß = \frac{d_i}{d_{Rk,i}}$
I	31.2	0.14
II	18.3	0.08
III	18.3	0.08
IV	18.0	0.08
V	18.3	0.08
VI	18.3	0.08

[a)]The reactor heights (h_{Rk}) include the reactor prechamber.

As pyrolysis is an endothermal reaction, the heat supply is decisive for the product gas composition.[56,57] Due to the TCL in the LMBCR (Figure 2), the reactor may be considered as an annular gap reactor. On the other hand, Al-Ou fi et al.[71] concluded that the annular gap character of a reactor affects bubble rise, if the gas void fraction ß is above 0.25. The impact of the annular gap character of a bubble column increases with increasing ß Equation (1).

$$ß = \frac{d_i}{d_{Rk,i}} \tag{1}$$

The outer diameter of the inside pipe (in case of this study the TCL) is $d_i$and the inner diameter of the bubble column is $d_{Rk,i}$. Al-Ou fi et al.[71] investigated systems with ß between 0.25 and 0.69, whereas in this study all ß values were found to be below 0.15 (Table 5).

With these small values of ß and the decrease in hydraulic inner diameter ($d_h = d_{Rk,i} - d_i$)[71] caused by the TCL is relatively small, the influence of the inner tube is neglected in this publication. Wall effects, however, cannot be excluded in general: Clift et al.[63] suggested a correction factor for the bubble rise velocity, which depends on the Eötvös number (Eo_B, Equation (2),[63]) and the Reynolds number (Re_B, Equation (3)[63]) of the bubbles at the moment of detachment from the orifice. Additionally, the ratio of the bubble diameter d_B to the reactor diameter $d_{RK,i}$ (λ, Equation (4),[63]) is needed.

$$Eo_B = \frac{\Delta\rho_{G;Sn} \times g \times {d_B}^2}{2 \times \sigma_{sn}} \tag{2}$$

$$Re_B = \frac{\rho_{Sn} \times u_B \times d_B}{\eta_{Sn}} \tag{3}$$

$$\lambda = \frac{d_B}{d_{RK,i}} \tag{4}$$

Clift et al.[63] concluded that for bubble diameters $d_B > 2$mm, $Eo_B < 40$, $Re_B > 200$ and $\lambda < 0.6$ small wall effects occur, which slow down the bubble rise velocity. The values of Eo_B and Re_B depend on the densities of the liquid tin ρ_{Sn} and the gas phase ρ_G the viscosity η_{Sn}, the surface tension $\sigma_{sn}$of the tin, and the bubble rise velocity u_B. The calculation of material properties is described in detail in Section 4.1, Supporting Information for the tin, and in Section 2, Supporting Information for the gas.

As the bubble diameter cannot be determined directly, a correlation proposed by Uhlenbruck et al.[72] was used for the estimation of residence times for liquid metal bubble columns. The calculation of the bubble diameter d_B is described in detail in the Section 4.3, Supporting Information of this publication. Examples are given in **Figure 5**.

In Figure 5, reactor type VI typifies all reactors with a height-to-diameter-ratio of 18.0–18.3 (Table 5): The geometry of reactor types II to VI shows the same inner diameters and the same orifice diameters. They differ in their prechamber volumes and orifice hole numbers. The influence of these properties was discussed in Section 2.6 and 2.8.

© 2024 The Author(s). Energy Technology published by Wiley-VCH GmbH

21944296, 0, Downloaded from https://onlinelibrary.wiley.com/doi/10.1002/ente.202400183 by Christoph Hofberger , Wiley Online Library on [16/07/2024]. See the Terms and Conditions (https://onlinelibrary.wiley.com/terms-and-conditions) on Wiley Online Library for rules of use; OA articles are governed by the applicable Creative Commons License

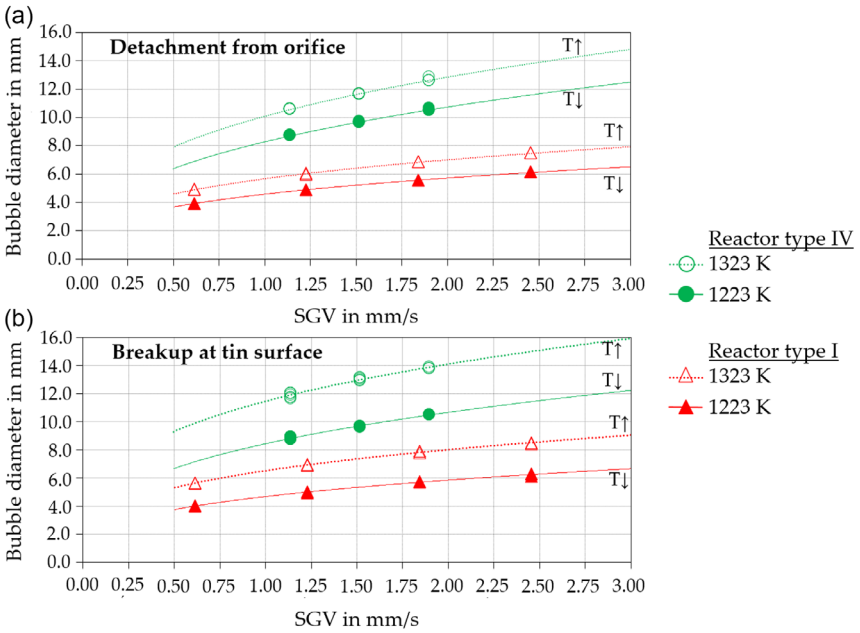

Figure 5. Comparison of the calculated bubble diameters at 1223 and 1323 K in LMBCR types I and IV without reactor prechambers. a) Compares the bubble diameters at bubble detachment from the orifice at several SGVs and temperatures of Reactor types I and IV. b) Compares the bubble diameters at the breakup at the tin surface several SGVs and temperatures of Reactor types I and IV. SGVs have accuracy $\geq\pm 0.013$ mm s^{-1} (according to GUM). The resulting uncertainty of the bubble diameter based on the measured values of this study is below 0.4 mm.

For these calculations, the volume increase of the bubble due to the pressure drop of the rising bubble and the changes in the amount of substance in the gas phase due to the pyrolysis reaction[56] are taken into account, as described in Section 4.5, Supporting Information. It can be seen that the bubble diameters d_B are strictly >2 mm. This leads, in addition to the determined values Eo_B Equation (2), Re_B Equation (3) and λ Equation (4) as mentioned earlier, to small wall effects. These conditions are present in all experiments.

According to a parameter study, the volume flow of the feed gas has the highest influence on the bubble diameter. If the volume flow of the LMBCR type IV is reduced to the values of LMBCR type I, calculations lead to comparable bubble sizes. The influence of the temperature is similarly high. For these calculations, the measured mean temperature of the tin is used as the temperature of the feed gas. Since Geißler et al.[59] concluded that the gas inside the bubble heats up quickly, this can be considered an acceptable approximation. On the one hand, the mean temperature is used in the correlation for several material properties of the tin (viscosity, density, and surface tension), on the other hand, the real volume flow of the gas is strongly affected by the temperature (assuming an ideal gas behavior). Finally, it can be assumed that at the given SGVs in LMBCR type IV, probably larger bubbles are formed than in LMBCR type I. The effects of several conditions and geometrics, determined in this parameter study, are summarized in **Table 6**.

On the other hand, it cannot be assumed that increased wall effects will occur due to increased bubble diameter, since the LMBCR type IV has an increased inner diameter as well. Clift et al.[63] proposes a correction factor $[1-\lambda^2]^{\frac{3}{2}}$ for the correction of the bubble rise velocity due to wall effects. The correction factors for all LMBCR types without reactor prechamber are listed in **Table 7**.

Table 6. By means of parameter study determined effects of conditions and reactor geometries on bubble diameter and rise velocity for the range of this survey.

Condition/geometry	Effect on	
	bubble diameter	bubble rise velocity
SGV ↑	↑	↑
Temperature ↑	↑	↑
LM density ↑	↓	↓
LM viscosity ↑	↑	↑
LM surface tension ↑	↑	↑
Gas phase viscosity ↑	No effect	No effect
Reactor diameter ↑	No effect	↓
Orifice diameter ↑	↑	↑

If the correction factor is 1, the wall effects are negligible. As predicted earlier, LMBCR type IV shows wall effects, despite its inner diameter is high. Nevertheless, the impact of all wall effects on the rise velocity is less than 7%. The calculation implies that the different geometries of the reactors relating to their inner diameters seem to have a small influence on bubbles and their rising behavior. However, since the inner diameters of the orifices are different and the volume flows seem to have a significant influence on the bubble size, this may also result in significant differences in the bubble regimes.

© 2024 The Author(s). Energy Technology published by Wiley-VCH GmbH

21944296, 0, Downloaded from https://onlinelibrary.wiley.com/doi/10.1002/ente.202400183 by Christoph Hofberger , Wiley Online Library on [16/07/2024]. See the Terms and Conditions (https://onlinelibrary.wiley.com/terms-and-conditions) on Wiley Online Library for rules of use; OA articles are governed by the applicable Creative Commons License

Table 7. Calculated correction factors for the bubble rise velocity in reactors without reactor prechambers.

LMBCR type RT	Tin temperature [K]	SGV (methane) [mm s^{-1}]	Initial correction factor $[1-\lambda^2]^{\frac{3}{2}}$	Tin surface correction factor $[1-\lambda^2]^{\frac{3}{2}}$
I	1193–1447	0.6	1.0	0.97–1.0
I	1193–1447	1.2	0.98–1.0	0.96–1.0
I	1193–1447	1.8	0.97–0.98	0.94–0.96
I	1193–1447	2.5	0.96–0.97	0.93–0.95
IV	1222–1431	1.1	1.0	0.96–0.97
IV	1222–1431	1.5	0.97–0.98	0.95–0.97
IV	1222–1431	1.9	0.97	0.93–0.96

2.4. Orifice and Bubble Regimes

According to Kulkarni et al.[73] several bubble formation regimes can occur: 1) Separated bubble regime, where the bubble detachment volume is constant and the frequency of bubble detachment is dependent on volume flow; 2) intermediate or chain regime, where the bubble detachment frequency is constant and the bubble detachment volume depends on volume flow. In this regime, various bubble formation processes can occur as single and multibubbling, or doublet coalescence for instance; and 3) jetting regime, where the gas leaves the orifice as a gas jet and the bubble formation results from the jet break-up.

The type of bubbling regimes occurring is strongly dependent on the Weber Equation (5)[74] and the Reynolds Equation (6) numbers of the orifice.

$$\mathrm{We_O} = \frac{\rho_G \times u_O^2 \times d_O}{\sigma_L} \tag{5}$$

$$\mathrm{Re_O} = \frac{\rho_G \times u_O \times d_O}{\eta_G} \tag{6}$$

Both $\mathrm{We_O}$ and $\mathrm{Re_O}$ numbers depend on the gas density ρ_G (Section 4.2, Supporting Information), the gas velocity (in the orifice) u_O, and the inner orifice diameter d_O. The orifice diameter of RT I is slightly different from that of all other LMBCR types. The manufacturer specified the hole diameters to be 0.5 ± 0.1 mm for RT I and 0.6 ± 0.1 mm RT II+. Four random samples (RT IV and RT V) were analyzed microscopically. The orifice diameters were found to range between 0.55 and 0.72 mm on the average. All holes were found to taper in depth. An example is given in **Figure 6**.

The dynamic gas viscosities η_G and the surface tensions of the tin σ_L are needed as well (Section 4.2, Supporting Information). All values, except for the inner orifice diameter, are strongly influenced by the tin temperature, which results in a similar value range of $\mathrm{We_O}$ and $\mathrm{Re_O}$ for all LMBCR types (**Figure 7**). The properties of tin were calculated, using the average tin temperature and the gas properties and the reactor prechamber or inlet temperature. For reactors with a three-hole orifice, it is assumed that the volume flow is evenly distributed between the orifice holes.

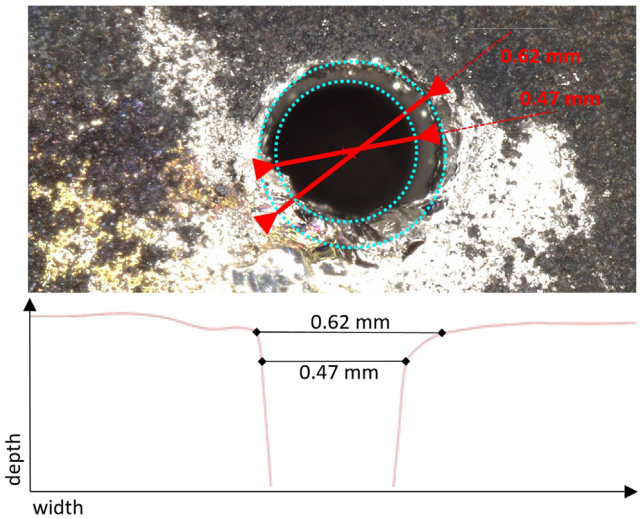

Figure 6. Example of an orifice of RT V after an experimental test series. White surface: quartz glass with tin layer; black surface: quartz glass with carbon layer.

According to Figure 7, higher SGVs or throughputs lead to higher $\mathrm{We_O}$ and $\mathrm{Re_O}$ numbers. The throughput in the form of the gas velocity in the orifice u_O is part of both equations for $\mathrm{We_O}$ (Equation (5)) and $\mathrm{Re_O}$ (Equation (6)). For the calculation of the gas velocity in the orifice, the reactor prechamber or inlet temperature was used. Temperature measurement is challenging: At tin temperatures between 1223 and 1473 K, thermal radiation may play an important role as the radiation reaches the visible spectrum[75] as illustrated in **Figure 8**.

The $\mathrm{Re_O}$ numbers calculated were found to be independent of the temperature. As $\mathrm{Re_O}$ Equation (6) contains several temperature dependent values (ρ_G and η_G Section 4.2, Supporting Information, u_O), the temperature influence is approximately cancelled out. $\mathrm{We_O}$ Equation (5) shows a low temperature dependence only.

Gas density that affects the values of both $\mathrm{We_O}$ and $\mathrm{Re_O}$ can be influenced not only by the temperature and pressure but also by the feed gas composition. The mixtures with the highest density difference to PM pyrolyzed for this study were MPM (1%, 5%, and 10% of propane). The $\mathrm{We_O}$ and $\mathrm{Re_O}$ numbers of MPM feed increase with rising density and propane amount (**Figure 9**).

These numbers seem to be influenced mainly by the density of the feed gas, defined by mixture and pressure (calculation described in the Section 4.2, Supporting Information). The resulting $\mathrm{We_O}$ numbers are between 0.03 and 2.3. Capponi et al.[74] define $\mathrm{We_O}$ numbers below 250 as low. These low $\mathrm{We_O}$ numbers are expected to result in single bubbling without pairing or coalescence. The Reynolds numbers confirm the suggestion of Camarasa et al.[76] of single bubbling behavior: all $\mathrm{Re_O}$ numbers from all experiments resulted in values between 93 and 945. Camarasa et al.[76] define Reynolds numbers between 100 and 2000 as the chain bubble regime. When considering the maximum resulting of $\mathrm{Re_O}$ and $\mathrm{We_O}$ due to hole geometry measurement uncertainties, all values of $\mathrm{Re_O}$ and $\mathrm{We_O}$ remain within these ranges. Since all reactors

© 2024 The Author(s). Energy Technology published by Wiley-VCH GmbH

21944296, 0, Downloaded from https://onlinelibrary.wiley.com/doi/10.1002/ente.202400183 by Christoph Hofberger , Wiley Online Library on [16/07/2024]. See the Terms and Conditions (https://onlinelibrary.wiley.com/terms-and-conditions) on Wiley Online Library for rules of use; OA articles are governed by the applicable Creative Commons License

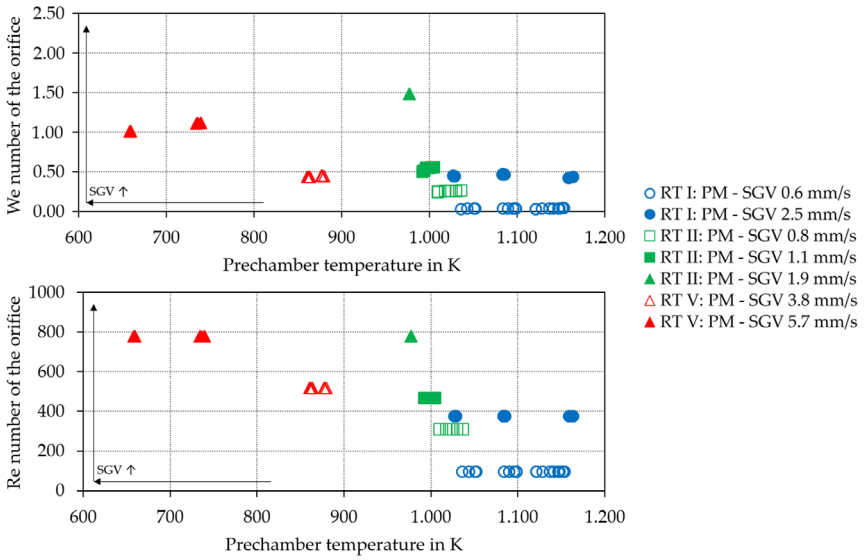

Figure 7. Comparison of Weber and Reynolds numbers of several reactor types with PM feed. The accuracy of the prechamber temperatures in accordance with GUM was found to be $\leq\pm15$ K.

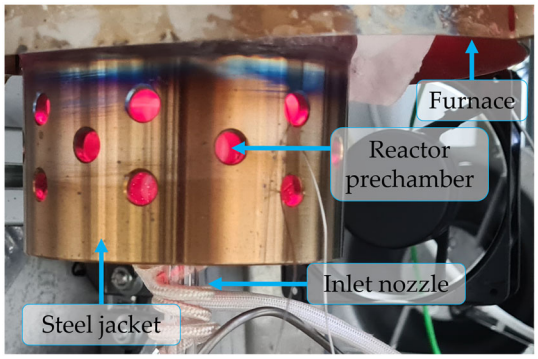

Figure 8. Visible thermal radiation in the reactor prechamber of LMBCR type VI.

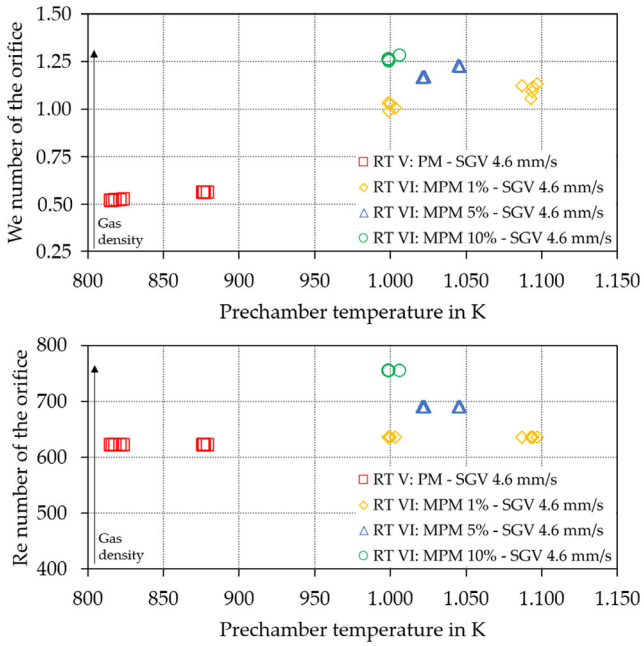

Figure 9. Comparison of Weber and Reynolds numbers of several LMBCR types with PM and a MPM. The accuracy of the prechamber temperatures in accordance with GUM: $\leq\pm15$ K.

show comparable bubble formation, the reactor designs are now examined about their influence the bubble rise behavior.

2.5. Residence Time

The bubble rise behavior has a major influence on the residence time and, thus, on conversion rates and yields.[56] As described in the Section 4.5, Supporting Information, the bubble diameter and rise velocity were calculated iteratively. Some representative results are summarized in **Figure 10**.

In RT I (Figure 10a), a clear dependence of the calculated bubble size on the SGV can be seen: a higher SGV leads to a shorter residence time. Although RT I with a SGV of 2.5 mm s^{-1} has the same throughput as RT II with a SGV of 0.8 mm s^{-1}, the residence time in RT II is further reduced compared to RT I. There are two reasons: first, the hole diameter of RT II is 0.1 mm larger on average than the hole diameter of RT I (RT I: 0.5 mm $\pm$ 0.1 mm; RT II: 0.6 mm $\pm$ 0.1 mm), and second, RT II has a significantly increased inner diameter, which reduces wall effects slowing down the rising bubbles. This suits well to the results summarized in Table 7: comparing RT I with RT IV (same inner diameter as RT II), wall effects occur in RT I at 2.5 mm s^{-1}, but not in RT IV at 1.1 mm s^{-1} (and below). In RT II, the tendency of RT I is continuing: increased SGVs lead to decreased residence times. RT V, on the other hand, does not show this effect. However, the comparison is not straightforward. In the calculations conducted in this case, the swarm effects of the

© 2024 The Author(s). Energy Technology published by Wiley-VCH GmbH

21944296, 0, Downloaded from https://onlinelibrary.wiley.com/doi/10.1002/ente.202400183 by Christoph Hofberger , Wiley Online Library on [16/07/2024]. See the Terms and Conditions (https://onlinelibrary.wiley.com/terms-and-conditions) on Wiley Online Library for rules of use; OA articles are governed by the applicable Creative Commons License

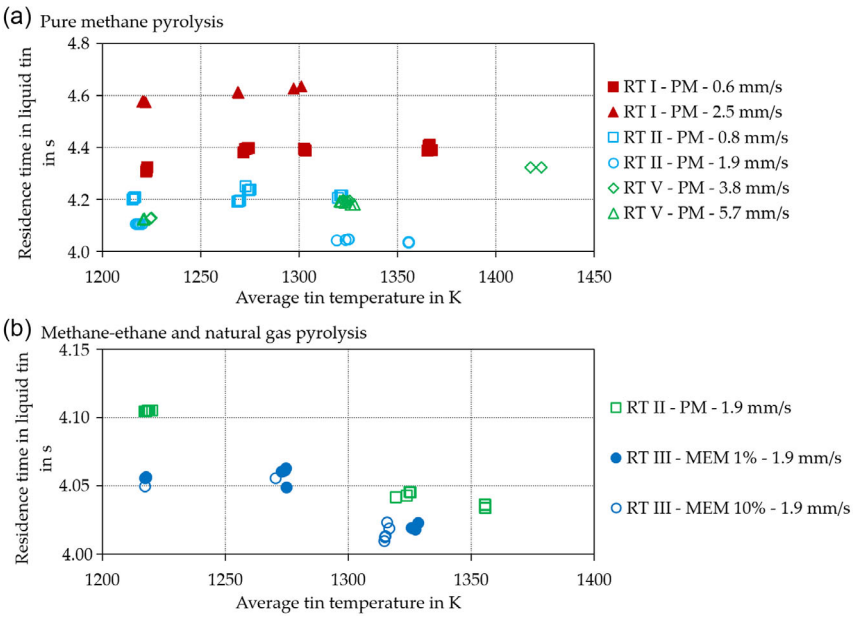

Figure 10. Overview of residence times of gas bubbles in liquid tin. a) Bubble residence time of PM pyrolysis. b) Bubble residence time of a MEM and nGH pyrolysis. Accuracy of the average tin temperatures: $\leq\pm15$ K, accuracy of the residence time of the bubble: $\leq\pm0.13$ s. Both in accordance with GUM.

rising bubbles are not taken into account. The calculations were carried out for one orifice hole each. Since RT V is constructed with a three-hole orifice, volume flow was presumed to be distributed equally between these three holes. In a comparison of the dispersion of different gases, only a weak dependence of the residence time on the incoming gas mixture could be observed. In all cases, it can be seen that the average tin temperature has no significant influence on the bubble residence time. Further effects on the residence time could be caused by the use of reactor prechambers.[77] It has been investigated experimentally, as prechambers can have various advantages in the handling of LM.[77]

2.6. Prechambers

Prechambers in general are defined as volumes between the pressure drop prior up stream of to the orifice plate and the orifice plate.[78] They are proposed to minimize pressure fluctuations at the reactor inlet which might lead to weeping events.[79] In the present case, weeping was defined as the liquid tin transport to the outside of the reactor, subsequently leading to inlet blockages, if the tin reaches parts of the reactor inlet system which are below solidification temperature of the tin.

A second advantage of prechambers is the resulting possibility to implement multihole dispersion without complicated changes in the periphery of the reactor vessel. However, according to this definition, several parts of the gas supply system must be included. The first pressure drop downstream of the mass flow controllers is caused by the static gas mixer. The whole gas flow through downstream volumes (pipes, tin collection vessel, reactor inlet nozzle, and reactor prechamber) has to be taken into account for the overall prechamber volume. For this reason, the LMBCR types in this study show high differences regarding the overall prechamber volume. The dimensionless prechamber volume number N''_C according to Equation (7) from Sano and Mori[77] compares the surplus gas accumulated in the gas chamber, to the bubble volume. The calculated values are summarized in **Table 8**. The dimensionless parameter N_W Equation (8) is needed to prove that the inertia force, the surface force, and the gravity force of the gas suits to the chosen correlation. This number is based on We_O (inertia force to surface force, Equation (5)) and Fr_O (inertia force to gravity force of the gas, Equation (9)).[77]

Table 8. Overall prechamber volumes and volume flow regimes according to Sano and Mori[77] of the experimental campaigns of this study.

Reactor type	N''_C	N_W	Prechamber volume regime	Gas flow regime	Feed gas mixture
I	51–74	4–17	Large	Low	PM
II	137–213	8–46	Large	Low	PM
III	351–490	16–50	Large	Low	MEM 1–15%
IV	52–69	24–46	Large	Low	nGH
V	282–491	13–26	Large	Low	PM
VI	188–213	25–40	Large	Low	MPM 1–15%

$$N''_C = \frac{4 \times V_C \times \rho_{Sn} \times g \times \sin(\theta)}{\pi \times d_{no}^2 \times p_S} \tag{7}$$

$$N_W = We_O \times Fr_O^{-0.5} \tag{8}$$

$$Fr_O = \frac{u_O^2}{d_O \times g} \tag{9}$$

© 2024 The Author(s). Energy Technology published by Wiley-VCH GmbH

21944296, 0, Downloaded from https://onlinelibrary.wiley.com/doi/10.1002/ente.202400183 by Christoph Hofberger , Wiley Online Library on [16/07/2024]. See the Terms and Conditions (https://onlinelibrary.wiley.com/terms-and-conditions) on Wiley Online Library for rules of use; OA articles are governed by the applicable Creative Commons License

As shown in Equation (7), the dimensionless prechamber volume N''_C depends on constant values such as the prechamber volume V_C, the inner orifice diameter d_{NO}, and the contact angle of tin to quartz glass θ, as well as on the variable values of the static pressure at the orifice p_S and the density of tin ρ_{Sn} (Section 4.1, Supporting Information). As ρ_{Sn} depends on the tin temperature and p_S on the gas volume flow and the reactor age (or time of pyrolysis), N''_C was not a constant value during the experiments.

The overall prechamber volumes with a resulting N''_C above 9 and $N_W < 2.4 \times (N''_C - 1)$ were suggested to be "large prechambers" with "low gas-flow rate".[77] According to Sano and Mori,[77] the resulting bubble diameter is independent of the prechamber volume. Hence, no correction of the bubble diameter and residence times is necessary. This criterion is suitable for all LMBCR types and experiments of this study. Irons et al.[78] observed the formation of bubble pairs for large prechambers, Mori et al.[77] even found bubble quartets. Multibubble formation happens if a detached bubble affects the formation of the following bubble.[80] As mentioned earlier, large prechambers have a constant pressure which in turn leads to a fluctuating volume flow through the orifice[70] due to the changing bubble pressure during formation and detachment[81] and in the trail of the detached bubble.[78] To prove multibubble formation, Oguz and Prosperetti[82] developed the critical volume flow criterion Equation (10).

$$Q_{crit} = \pi \times \left(\frac{16}{3 \times g^2}\right)^{\frac{1}{6}} \times \left(\frac{\sigma_L \times d_O}{2 \times \rho_L}\right)^{\frac{4}{5}} \tag{10}$$

If the volume flow per orifice is above Q_{crit}, multibubble formation is probable. According to Equation (10), all experiments are in the multibubbling regime. In contradiction to Camarasa et al.[76] and Capponi et al.[74] the consideration of a large prechamber and the critical volume flow criterion of Oguz and Prosperetti[82] leads probably to multibubble formation. As the criterions of Camarasa et al.[76] and Capponi et al.[74] do not take a prechamber into account and all reactors are found to have large prechambers, multibubble formation seems more probable.

As mentioned earlier, gas temperature at the reactor inlet or in the reactor prechamber can also influence bubble formation, as it affects the real volumetric flow. The measured gas temperature depends on several obvious conditions, such as the tin average temperature and the gas volume flow (**Figure 11**).

The measured reactor prechamber temperatures of RT I and RT II suggest an average temperature (10 mm below the orifice) of 83% of the average tin temperature with a standard deviation of ±4%. Both RT I and RT II exhibit an inlet or reactor prechamber temperature dependence on the inlet gas flow: An increased gas flow results in decreased temperature. As the gas flow was not heated, the decreasing temperature can be explained by an increased cold gas flow. The dependence of the measured inlet temperature of RT I on the average tin temperature was difficult to prove. The first measurements of the experiment (Figure 11, LMBCR type I; Tin average temperatures 1223, 1273, and 1300 K) show a clear tendency: increased tin average temperatures lead to increased inlet temperatures. The data points at 1300 K show a significant drop of the measured inlet temperature. However, starting from this point, the tendency is fulfilled again. Increased average tin temperatures lead to increased inlet temperatures. The shift of the measured reactor inlet temperature (Figure 11, LMBCR type I) was caused by a weeping event.

The relation of the inlet temperature to the average tin temperature could be seen at all experiments, but the values can only be compared within the same experiment and under equal conditions, due to deviations of the thermocouple position or due to weeping which can affect the measurement results. The measured values are approximately the same. Since the gas flow conditions in the reactor prechamber are unknown (vortexes, dead zones, and the resulting temperature distribution), it is not possible to prove whether the measured temperature is only valid at certain points or can be assumed to be the average temperature in the reactor prechamber or reactor inlet. Dhotre et al.[83] conducted simulations of a bubble column containing a prechamber with a multihole orifice. These simulations reveal vortexes in the edge region of the multi-hole orifice in the prechamber.

As described earlier, significant effects of thermal radiation on the measured temperature can also be expected at the high tin temperatures achieved. In the experiments, pronounced incandescent phenomena occur at temperatures of 1000 K and higher. Weeping can also have a massive influence.

In agreement with Peng et al.[79] and Thorat et al.[64] this study demonstrated that the reactor prechamber of this reactor design did not prevent weeping. On the other hand, reactors with prechambers tolerated weeping better than reactors without prechambers: In the reactor with a tin weeping chamber, accumulated tin from the reactor prechamber or inlet nozzle could be transferred easily to the weeping chamber by heating the inlet nozzle during pyrolysis. This results in a much longer reactor

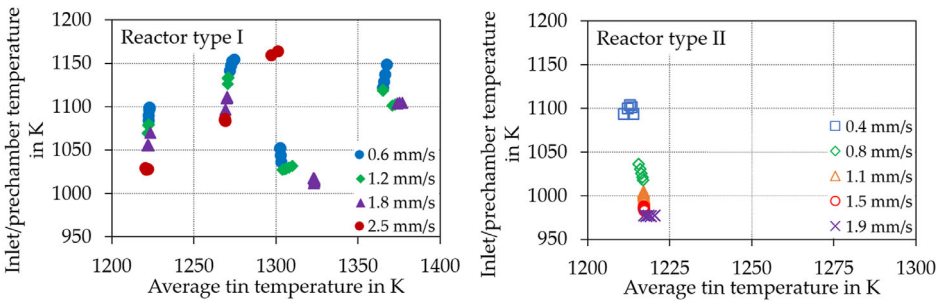

Figure 11. Comparison of measured reactor inlet temperatures with the average tin temperature of two LMBCR types for PM pyrolysis. Accuracy of all temperatures in accordance with GUM: ≤±5%.

© 2024 The Author(s). Energy Technology published by Wiley-VCH GmbH

21944296, 0, Downloaded from https://onlinelibrary.wiley.com/doi/10.1002/ente.202400183 by Christoph Hofberger , Wiley Online Library on [16/07/2024]. See the Terms and Conditions (https://onlinelibrary.wiley.com/terms-and-conditions) on Wiley Online Library for rules of use; OA articles are governed by the applicable Creative Commons License

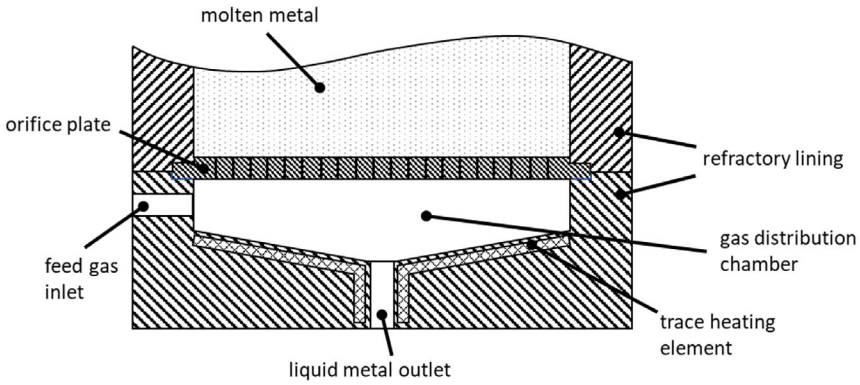

Figure 12. Exemplary design of the gas supply for a large scale reactor.

life time and a more controllable system. For this reactor design, reactor prechambers are required anyway to implement multihole dispersion. Since weeping is a process that cannot be avoided completely by using orifice plates as dispersion units[64,79,84,85] (except forcing jetting regime for bubble formation[84]), the combination of a reactor prechamber with a tin weeping chamber is highly recommended.

These findings can be used in the future for the design of a reactor on a commercial scale. **Figure 12** shows how the lower part of the reactor, including the gas distribution chamber and the orifice plate, could be designed.

The reactor consists of a metallic pressure jacket (not shown in the Figure 12) and is lined with refractory material inside. The refractory material is in direct contact with the molten metal. Below the molten metal, the orifice plate is located. It is provided with a large number of openings through which the gas is finely dispersed into the molten metal. The gas distribution chamber is located below the orifice plate. Depending on the process conditions, penetration of liquid metal from the upper area of the bubble column through the orifices into the gas distribution chamber cannot be ruled out. Contrary to the design in the experimental set-up, the gas in a technical scale apparatus would be introduced laterally into the distribution chamber to prevent clogging of the gas supply line by molten metal. To facilitate the outflow of the penetrated liquid metal from the gas distribution chamber, the bottom of the gas distribution chamber is designed to slope down toward the outlet for the liquid metal in the middle. In order to ensure that the outflowing molten metal does not solidify and clog of the gas distribution chamber or the liquid metal outlet, the liquid metal outlet and the bottom of the gas distribution chamber are provided with a trace heating system. To prevent gas slip through the liquid metal outlet, the downstream flow channel is designed as a siphon with an additional valve.

Since the orifice plate above the gas distribution chamber is subject to high mechanical loads, it can be supported by a metal grid to be installed underneath, which absorbs some of the forces. This prechamber concept, combined with high volume flows, is expected to have positive effects on the reactor lifetime.

Within this study, higher volume flows led to less weeping. In addition to weeping, pyrolysis in the reactor prechamber can lead to clogging and shorten the lifetime of the pyrolysis reactors due to carbon formation. Above 1073 K,[86] methane

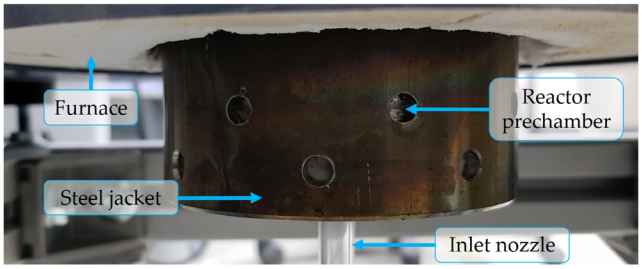

Figure 13. Improved reactor prechamber cooling system: perforated steel jacked.

pyrolysis proceeds with significant conversion rates with a feed gas composition containing higher hydrocarbons even at lower temperatures.[57] When these gas temperatures are reached in the reactor prechamber, undesirable pyrolysis occurs. There are two ways to counteract the formation of carbon without changing the feed gas composition: first by reducing the residence time in the reactor prechamber and second by reducing the temperature of the reactor prechamber. The reduction of the residence time can be achieved mainly by increasing the flow rate. This can also lead to a lower temperature due to the higher amount of cold gas streaming into the prechamber. Nevertheless, the reduction of the reactor prechamber temperature is achieved mainly by active cooling. From the design point of view, the steel jacket containing the quartz glass reactor was perforated along the height of the reactor prechamber (**Figure 13**). Additionally, a ventilation system was installed.

This combined method has significantly reduced pyrolysis in the prechamber. As weeping and prechamber or inlet pyrolysis are controllable by the methods described in this section, these processes occur during normal operation. Weeping in particular was observed to become more frequent under unstable conditions when filling the reactor with liquid tin, for example. In order to prevent weeping, this process has to be considered and designed precisely.

2.7. Weeping

The highly purified tin (>99.5%) used for the experiments of this study was available in the form of granules (diameter of 2–4 mm)

© 2024 The Author(s). Energy Technology published by Wiley-VCH GmbH

21944296, 0, Downloaded from https://onlinelibrary.wiley.com/doi/10.1002/ente.202400183 by Christoph Hofberger , Wiley Online Library on [16/07/2024]. See the Terms and Conditions (https://onlinelibrary.wiley.com/terms-and-conditions) on Wiley Online Library for rules of use; OA articles are governed by the applicable Creative Commons License

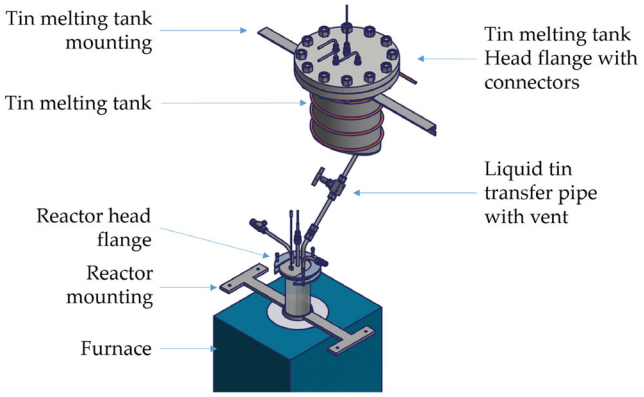

Figure 14. Tin melting tank and its position above the LMBCR in the furnace.

and pellets (≈10 × 5 mm). Due to the lower bulk density of both compared to liquid tin, the tin was melted in a tin melting vessel and transferred in liquid state to the reactor. The tin melting tank was placed above the reactor and connected to the reactor head flange (**Figure 14**).

During the reactor filling process, a gas volume flow through the reactor orifice is necessary to prevent tin from entering reactor inlet or reactor prechamber. The filling state of the reactor could be estimated by height-dependent temperature values, measured by the TCL and the static inlet gas flow pressure.[56] The solidified tin from previous experiments could be melted and reused. After being recycled twice, the tin contained up to 0.4% chromium and 0.8% nickel, as measured using energy-dispersive X-ray spectroscopy. Additionally, small areas with increased aluminum content (up to 4%) could be determined. The melting tank could be the source of the impurities, as the material contained between 6% and 8% chromium and 0.5% and 1% aluminum. The source of the nickel probably was the liquid tin transfer pipes and vents that contained between 9% and 12% nickel (Stainless steel 316/316L. Values published from Swagelok. Current status 26.09.2023.). Tin handling is not only relevant to the start-up of the reactor but also to its operation.

In bubble columns, weeping is a well-known process investigated in a broad range of bubble column applications.[64,84,87–90] The force driving this process is the fluctuation of the pressure difference between both sides of the orifice.[89] Peng et al.[79] concluded that weeping occurs immediately after bubble detachment as a rebound of the liquid phase into the orifice. They found that the intensity of the weeping depends not only on the gas velocity and orifice diameter but also on the flow and bubbling regime of the gas.[76] According to Camarasa et al.[76] at low volume flows in the constant volume bubbling regime, the formed bubbles are small which leads to low weeping intensity. With increasing volume flow, the bubbling regime of constant frequency is reached, where the bubble diameter is increasing. Higher bubble diameter leads to more weeping. If the volume flow is further increased, the bubble formation enters the jetting regime, where the weeping intensity is decreasing.[76] The static pressure and therefore smaller bubbles also influences the weeping behavior. As mentioned before, weeping depends on the bubble diameter.[76] The bubble diameter depends on the liquid metal capacities as well. Also the temperature and purity of the liquid metal show effects on the weeping behavior.[73,91]

Depending on the system and relative to the gas velocity, weeping shows minimal intensities at low and high (jetting) volume flows and maximal intensities at moderate volume flows.[85] Prechambers can minimize pressure fluctuations during bubble formation and decrease weeping intensity,[79] but in general weeping is a nonpreventable process, if the bubble formation is outside of the jetting regime.[85,90] If the bubbling regime is beyond the jetting regime, which it was for all RTs and experiments of this study, weeping in form of a spray mist was consistently present. It is an omnipresent process that occurs as part of bubble formation in bubble columns.[64,79,84,85,89,90] Furthermore, sudden pressure drops in the inlet system, as well as pressure peaks in the reactor head, lead to abrupt weeping events. These events can lead to clogging in the reactor inlet and to the accumulation of tin adhesions in the inlet or the reactor prechamber (**Figure 15**a,c).

Sudden tin weeping could be prevented effectively by head pressure control and reactor inlet pressure control. The head pressure was controlled consistently for LMBCR types IV, V, and VI. The reactor inlet pressure control was activated only, if the inlet pressure due to the adjusted gas mass flow exceeded 3 bars(a). In this case, the mass flow controllers were switched off. Then, bubble dispersion was operated only by the inlet pressure controller. The tin mist, in the nozzle or reactor prechamber (Figure 15b,d), still occurred for every gas flow and reactor

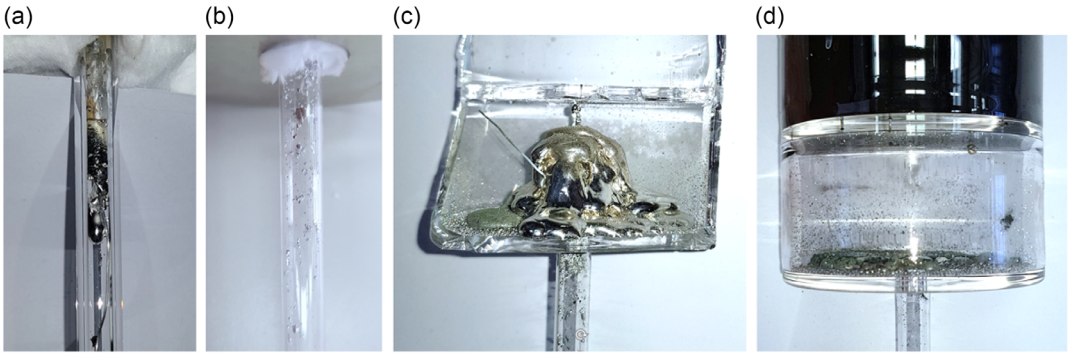

Figure 15. Reactors without reactor prechambers: Inlet nozzles a) after a sudden weeping event and b) with adhered weeping mist; reactor prechambers c) after sudden a weeping event and d) with adhered weeping mist.

© 2024 The Author(s). Energy Technology published by Wiley-VCH GmbH

21944296, 0, Downloaded from https://onlinelibrary.wiley.com/doi/10.1002/ente.202400183 by Christoph Hofberger , Wiley Online Library on [16/07/2024]. See the Terms and Conditions (https://onlinelibrary.wiley.com/terms-and-conditions) on Wiley Online Library for rules of use; OA articles are governed by the applicable Creative Commons License

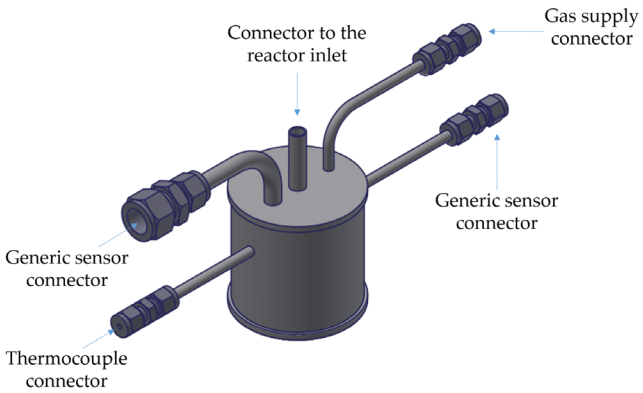

Figure 16. Illustration of the tin collecting vessel developed.

geometry when both controllers were activated. The tin adhesions in the inlet nozzle or reactor prechamber as illustrated in Figure 15b and c would clog the reactor inlet, if they were not removed. Consequently, the reactor nozzle was equipped with a heating system to melt the adhered tin. In addition, a tin collecting vessel (**Figure 16**) was installed between the reactor inlet nozzle (Figure 2) and the gas supply system.

The tin collecting vessel was constructed as a separator to collect the molten tin without affecting the feed gas flow. In combination with the inlet heating system, this approach to overcoming weeping blockades was tested successfully several times. The effect of removing adhered tin mist particles from the reactor inlet may be enhanced by weeping events by means of pressure drops with pure N_2 feed gas flow. **Figure 17** illustrates the effect of the inlet nozzle flushing procedure in three stages.

In Figure 17a, the inlet nozzle is partly blocked with tin. When the inlet pressure is reduced below the static pressure of the tin, massive tin weeping happens. It does not solidify in the nozzle due to high heating (Figure 17b). After this procedure, the tin in the nozzle is detached (Figure 17c) and passed to the tin collecting vessel.

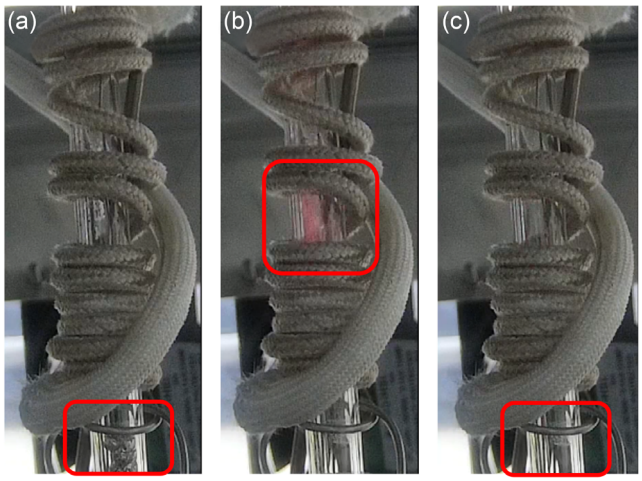

Figure 17. Inlet nozzle flushing procedure: a) Inlet nozzle with adhered tin. b) Inlet pressure drop induced weeping. c) Tin adherences were removed successfully.

By means of the procedures described in this section, sudden weeping events can be suppressed effectively and weeping-induced adhesions can be removed from the inlet during operation. Furthermore, reactors with prechambers were found to tolerate tin deposits due to the omnipresent weeping much longer before an intervention is necessary.

An additional lifetime-limiting process is carbon powder accumulation in the reactor head, as no carbon removal strategy was implemented in RT I to IV.

2.8. Carbon Management

Since large amounts of carbon are produced during the experiments, this carbon powder has to be removed during operation. In this study, two principles were selected: "passive-pneumatic discharge" and "passive flotation gravity discharge". Basically, both principles consist of a main gas line and a separate analysis gas line. Most of the product gas flows through the main gas line which is optimized for a low pressure drop. The carbon should be removed from the reactor using this line. The carbon dust is fed into a gravity separator to spate the powder from the gas flow. Downstream of the gravity separator, the gas stream is filtered in fine filters. Additionally, a pre-pressure controller keeps the product gas system (PGS) including the reactor head, pressurised at a defined value. The overpressure ensures that the analysis gas line is (passively) supplied with a product gas flow. In the case of the tested first principle (passive-pneumatic discharge, **Figure 18**a), the main product gas line is designed such that it causes a low pressure loss and, thus, discharges most of the product gas flow, but additionally leads to a gas velocity, sufficiently high to carry the carbon particles out of the reactor head. The carbon particles are then removed by means of the product gas flow. The second design tested (passive flotation gravity discharge) was a massively enlarged main product gas pipe diameter (to the inner diameter of the reactor). Carbon floating on the liquid tin piles up until it falls through the pipe bend into the carbon separator (Figure 18b).

The passive-pneumatic carbon removal method was found to be partly successful. Approximately 30 vol% of the produced carbon powder was removed, until the reactor head was filled with carbon and the product gas pipe was blocked. N_2 flow rates of up to 2000 $mL_N\ min^{-1}$ and pressure surges of up to 2 bar(a) into the reactor head caused additional carbon dust to be transferred. However, the reactor head could not be emptied.

Passive flotation gravity carbon discharge resulted in a significantly longer operating time. Carbon discharge using this technique was tested in RT VI. After 5.7 h of pyrolysis, the first carbon powder reached the gravity separator. This time was needed to fill the reactor head with a loose carbon fill (about 25 g) under the given process conditions. To prevent clots probably formed by pyrolysis reactions in the reactor head, the capacity of heating zone 3 (upper heating zone) was reduced, and the reactor head was equipped with an improved cooling system. Several service inlets (Figure 18) were intended for further experiments, injecting quench gas streams or execute mechanical operations in the reactor head. Anyhow the gravity separator was filled with carbon powder several times and successfully removed, emptied, and reattached during operation

© 2024 The Author(s). Energy Technology published by Wiley-VCH GmbH

21944296, 0, Downloaded from https://onlinelibrary.wiley.com/doi/10.1002/ente.202400183 by Christoph Hofberger , Wiley Online Library on [16/07/2024]. See the Terms and Conditions (https://onlinelibrary.wiley.com/terms-and-conditions) on Wiley Online Library for rules of use; OA articles are governed by the applicable Creative Commons License

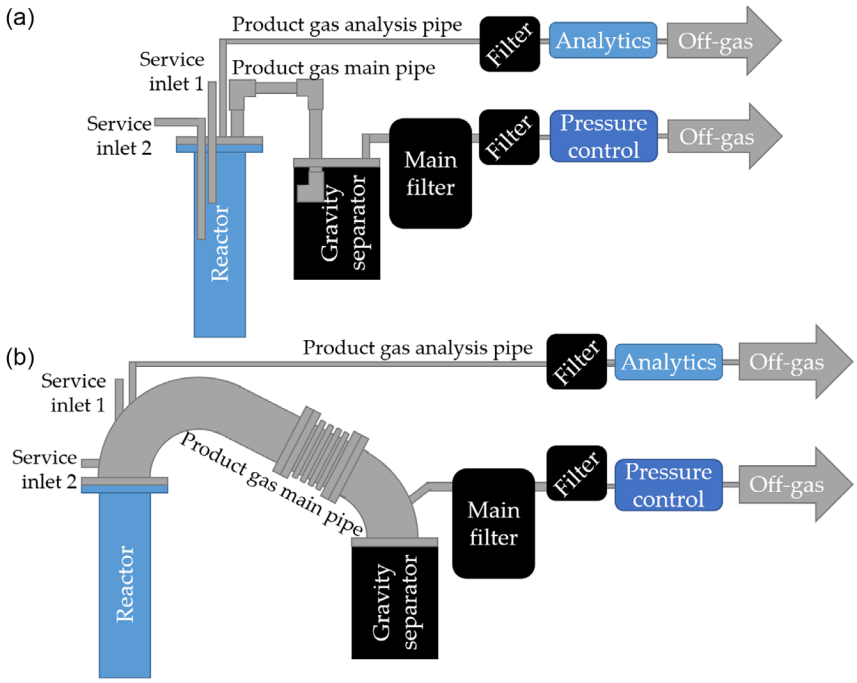

Figure 18. Schematic illustration of the tested carbon removal methods. Both systems feature an active head pressure control and an analysis gas line with a minimised dead volume a) Passive pneumatic carbon removal through the feed gas stream. b) Passive flotation discharge.

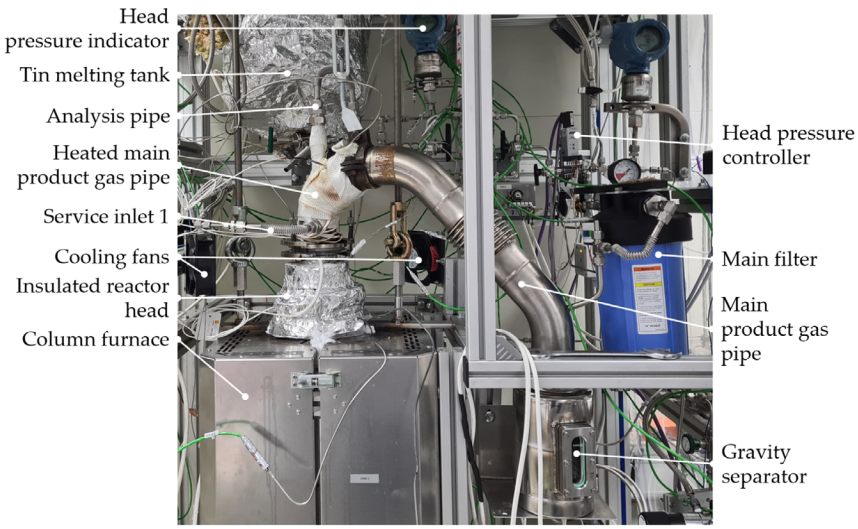

Figure 19. Reactor system with passive flotation carbon discharge, gravity carbon separator, and PGS pressure control in the highest expansion stage.

(pure N_2 feed). The lower part of the main product gas pipe was thermally insulated and could be heated to prevent tin accumulations due to the bubble breakup on the liquid tin surface (**Figure 19**).

3. Conclusions

Based on the LMBCR technology developed at KIT by Geißler et al.[52,58,59] the pyrolysis system could be scaled up[56] and further developed to ensure long-term operation. Since this technology was also found to be suitable for nGH feed recently,[57] the aim of this study was to investigate and characterize individual system units with respect to their impact on pyrolysis and long-term operability. Based on this study, recommendations are being made for the development of a pilot-scale system.

The correlations used for the comparison between the fluid-dynamical characteristics of the LMBCR types revealed that the effects regarding the scale-up on bubble dynamics and therefore residence times are marginal. The bubble formation behavior

© 2024 The Author(s). Energy Technology published by Wiley-VCH GmbH

21944296, 0, Downloaded from https://onlinelibrary.wiley.com/doi/10.1002/ente.202400183 by Christoph Hofberger , Wiley Online Library on [16/07/2024]. See the Terms and Conditions (https://onlinelibrary.wiley.com/terms-and-conditions) on Wiley Online Library for rules of use; OA articles are governed by the applicable Creative Commons License

depends mostly on the geometry of the orifice and the volume flow. Wall effects play a negligible role, which is why the increasing effect of higher bubble diameters on the bubble rise velocity is not expected to be decreased. On the other hand, a higher reactor diameter should not lead to higher bubble rise velocities. Multihole dispersion was found to be a suitable method to increase the throughput while keeping the fluid mechanical characteristics of the bubble formation uncharged.

Due to the lack of correlations suitable for liquid tin, the bubble rise behavior could only be characterized under various simplifications (e.g., no coalescence effects, no bubble decay, and defined orifice geometry). When scaling the system up to the pilot scale, a variation of the dispersion holes per reactor area should be investigated. With regard to the influence of the reactor prechamber on bubble formation, the correlations used provided contradictory statements (e.g., single bubble, multiple bubble formation). Fundamental minimization of weeping could not be confirmed. In practice, active cooling and high (cold) feed gas mass flows were needed to prevent pyrolysis in the prechamber. Still, the utilization of a reactor prechamber is recommended: the investigated prechambers showed some decisive advantages. Prechambers were able to cope with both omnipresent and sudden weeping. During operation, the accumulated tin could also be melted by active heating and transferred from the reactor inlet area or prechamber to a tin collection vessel. A combination of the reactor prechamber with a collection chamber was therefore recommended for a scale-up. Additionally, prechambers are the easiest way to implement multihole dispersion.

As mentioned earlier, weeping cannot be prevented in principle. Anyhow, it should be further minimized by active inlet pressure control. Therefore, it should be possible to replace mass flow controlled feed by pressure controlled feed (in combination with volume flow measurement). This may also stabilize the reaction conditions.

For a pilot plant, an additional substantial increase in the volume flow should be examined. This increase should be high enough to reach jetting regime in bubble formation: On one hand, it can be examined if it is possible to prevent weeping completely. On the other hand, the impact on the conversion can be examined. A massive throughput increase is important for this technology: At the current throughput-to-tin ratio, a pilot plant with a throughput of 1000 kg methane per day (24 h) requires 19 tons of liquid tin. This would correspond to a reactor diameter of 2 m assuming the same filling level of the reactor. This ratio can be massively reduced by throughput increase toward jetting regime. Certainly, reaching the jetting regime should lead to decreased residence time and thus achievable conversion.[56] In future studies, it should be reviewed, if the increased throughput balances the expected decreased conversion. Regarding the impact of jetting regime, prechambers, and multihole orifice, there is a lack of knowledge about the effects on residence time. As minimal impurities (saluted and dispersed) affect surface tension and contact angle, it is expedient to determine the real values experimentally.[69] The flow conditions and temperature distribution in the prechamber are not understood likewise. To assess these prechamber flow characteristics, a computational fluid dynamics simulation seems to be beneficial.

The experiments demonstrated that increasing the volume flow leads to increased inlet pressure. In the present case, the reactor system was limited toward pressure tolerance. For future projects, finding construction materials to replace the quartz glass is indispensable to enhance pressure and therefore throughput.

The head pressure control was not only able to complement the reaction control but also proved to be advantageous for the removal of the resulting carbon from the reactor head. In this study, a passive discharge proved to be effective. The main product gas line was enlarged to the reactor diameter and discharged vertically downward. As the carbon build-up floats on top of the tin, the carbon falls through the main product gas line and is collected in a gravity separator. To minimize the dead time for product gas measurements, gas for analysis should be discharged directly from the reactor head with low volume flow. The volume flow in the analysis gas line can be adjusted by the head pressure control. These experience reasoned recommendations can be incorporated into the development of a pilot scale system, facilitating long-term operability. Finally, for future studies, precise carbon analytics are recommended. Therefore, pyrolysis experiments should be designed to resolve dependencies of the carbon purity and modification on process conditions. For further developments toward industrial application, carbon purification methods should be determined and discussed.

Acknowledgements

The authors sincerely thank Wintershall Dea for the cooperation between Winterhall Dea AG and KIT, exchange of ideas, and the financial support. The authors acknowledge support by the KIT-Publication Fund of Karlsruhe Institute of Technology.

Open Access funding enabled and organized by Projekt DEAL.

Conflict of Interest

The authors declare no conflict of interest.

Author Contributions

All authors have read and agreed to the published version of the manuscript.

Data Availability Statement

The data that support the findings of this study are available from the corresponding author upon reasonable request.

Keywords

bubble column, hydrogen production, liquid metals, pyrolysis

Received: January 29, 2024
Revised: June 11, 2024
Published online:

[1] H. Tropsch, G. Egloff, *Ind. Eng. Chem.* **1935**, *27*, 1063.
[2] G. M. Badger, *Progr. Phys. Org. Chem.* **1965**, *3*, 1.

© 2024 The Author(s). Energy Technology published by Wiley-VCH GmbH

21944296, 0, Downloaded from https://onlinelibrary.wiley.com/doi/10.1002/ente.202400183 by Christoph Hofberger , Wiley Online Library on [16/07/2024]. See the Terms and Conditions (https://onlinelibrary.wiley.com/terms-and-conditions) on Wiley Online Library for rules of use; OA articles are governed by the applicable Creative Commons License

[3] R. K. AS Gordon, in *Pyrolysis of Organic Compounds in the Gas Phase*, Government Printing Office **1968**.
[4] S. R. Patlolla, K. Katsu, A. Sharafian, K. Wei, O. E. Herrera, W. Mérida, *Renewable Sustainable Energy Rev.* **2023**, *181*, 113323.
[5] M. McConnachie, M. Konarova, S. Smart, *Int. J. Hydrogen Energy* **2023**, *48*, 25660.
[6] F. S. de Carvalho, L. C. B. dos Santos, P. T. Lacava, F. H. M. de Araújo, J. A. de Carvalho, *Energies* **2023**, *16*, 839.
[7] A. Çelik, I. B. Othman, H. Müller, P. Lott, O. Deutschmann, *React. Chem. Eng.* **2024**, *9*, 108.
[8] G. Wang, Y. Dai, H. Yang, Q. Xiong, K. Wang, J. Zhou, Y. Li, S. Wang, *Energy Fuels* **2020**, *34*, 15557.
[9] T. Y. A. Fahmy, Y. Fahmy, F. Mobarak, M. El-Sakhawy, R. E. Abou-Zeid, *Environ. Dev. Sustainability* **2020**, *22*, 17.
[10] K. Zeng, X. Yang, Y. Xie, H. Yang, J. Li, D. Zhong, H. Zuo, A. Nzihou, Y. Zhu, H. Chen, *Fuel* **2021**, *302*, 121103.
[11] T. Maqsood, J. Dai, Y. Zhang, M. Guang, B. Li, *J. Anal. Appl. Pyrolysis* **2021**, *159*, 105295.
[12] M. S. Qureshi, A. Oasmaa, H. Pihkola, I. Deviatkin, A. Tenhunen, J. Mannila, H. Minkkinen, M. Pohjakallio, J. Laine-Ylijoki, *J. Anal. Appl. Pyrolysis* **2020**, *152*, 104804.
[13] C. Palmer, E. Bunyan, J. Gelinas, M. J. Gordon, H. Metiu, E. W. McFarland, *Energy Fuels* **2020**, *34*, 16073.
[14] D. Kang, N. Rahimi, M. J. Gordon, H. Metiu, E. W. McFarland, *Appl. Catal. B: Environ.* **2019**, *254*, 659.
[15] J. Zeng, M. Tarazkar, T. Pennebaker, M. J. Gordon, H. Metiu, E. W. McFarland, *ACS Catal.* **2020**, *10*, 8223.
[16] Y. Ji, C. Palmer, E. E. Foley, R. Giovine, E. Yoshida, E. Sebti, A. R. Patterson, E. McFarland, R. J. Clément, *Carbon* **2023**, *204*, 26.
[17] M. S. Khan, B. L. Crynes, *Ind. Eng. Chem.* **1970**, *62*, 54.
[18] O. Olsvik, O. A. R. Holmen, *Chem. Eng. Technol.* **1995**, *18*, 349.
[19] V. Kevorkian, C. E. Heath, M. Boudart, *J. Phys. Chem.* **1960**, *64*, 964.
[20] G. I. Kozlov, V. G. Knorre, *Combust. Flame* **1962**, *6*, 253.
[21] H. B. Palmer, T. J. Hirt, *J. Phys. Chem.* **1963**, *67*, 709.
[22] C.-J. Chen, M. H. Back, R. A. Back, *Can. J. Chem.* **1975**, *53*, 3580.
[23] M. Steinberg, *Int. J. Hydrogen Energy* **1998**, *23*, 419.
[24] S. Rodat, S. Abanades, J. Coulié, G. Flamant, *Chem. Eng. J.* **2009**, *146*, 120.
[25] G. Fau, N. Gascoin, P. Gillard, J. Steelant, *J. Anal. Appl. Pyrolysis* **2013**, *104*, 1.
[26] V. S. Arutyunov, V. I. Vedeneev, *Russ. Chem. Rev.* **1991**, *60*, 1384.
[27] R. W. Marek, M. L. Pearce, in *Some Observations on the Kinetics of the Pyrolysis of Methane in a Fluidized-Bed Reactor*, Speer Carbon Co., Niagara Falls, NY **1967**, p. 5.
[28] R. J. Heaston, in *Investigation of Methane, Methane-Steam Reactions in an Argon Arc Plasma*, The Ohio State University, Ann Arbor, Michigan **1964**.
[29] S. Schneider, S. Bajohr, F. Graf, T. Kolb, *ChemBioEng Rev.* **2020**, *7*, 150.
[30] A. Bode, C. Anderlohr, J. Bernnat, F. Flick, F. Glenk, D. Klingler, G. Kolios, F. Scheiff, A. Wechsung, M. Hensmann, *Bundesministerium für Bildung und Forschung, Bonn* **2018**.
[31] *New process for clean hydrogen. BASF Research Press Conference on January*, **2019**.
[32] N. Muradov, *Int. J. Hydrogen Energy* **2001**, *26*, 1165.
[33] N. Muradov, F. Smith, C. Huang, A. T. Raissi, *Catal. Today* **2006**, *116*, 281.
[34] T. I. Korányi, M. Némethrea Beck, A. Horváth, *Energies* **2022**, *15*, 6342.
[35] J. R. Fincke, R. P. Anderson, T. A. Hyde, B. A. Detering, *Ind. Eng. Chem. Res.* **2002**, *41*, 1425.
[36] M. Dors, H. Nowakowska, M. Jasiński, J. Mizeraczyk, *Plasma Chem. Plasma Process.* **2014**, *34*, 313.
[37] S. J. Cassady, R. Choudhary, V. Boddapati, N. H. Pinkowski, D. F. Davidson, R. K. Hanson, *Int. J. Chem. Kinet.* **2020**, *52*, 725.
[38] S. I. Galanov, A. G. Zherlitsyn, Y. V. Medvedev, O. I. Sidorova, V. P. Shiyan, *Russ. J. Appl. Chem.* **2011**, *84*, 997.
[39] J. V. Medvedev, A. G. Levashkin, D. V. Sorochan, in *Carbon, Hydrogen Production Technology from Natural Gas*. Tomsk State University, Tomsk, Russia **2018**.
[40] A. A. M. Parra, D. W. Agar, *Int. J. Hydrogen Energy* **2017**, *42*, 13641.
[41] A. G. Fernández, J. Gomez-Vidal, E. Oró, A. Kruizenga, A. Solé, L. F. Cabeza, *Renewable Energy* **2019**, *140*, 152.
[42] L. Heller. **2013**. Literature review on heat transfer fluids, thermal energy storage systems in CSP plants. STERG Report.
[43] M. T. Islam, N. Huda, A. B. Abdullah, R. Saidur, *Renewable Sustainable Energy Rev.* **2018**, *91*, 987.
[44] M. Msheik, S. Rodat, S. Abanades, *Energy* **2022**, *260*, 124943.
[45] A. Heinzel, W. Hering, J. Konys, L. Marocco, K. Litfin, G. Müller, J. Pacio, C. Schroer, R. Stieglitz, L. Stoppel, *Energy Tech* **2017**, *5*, 1026.
[46] M. Msheik, S. Rodat, S. Abanades, *Energies* **2021**, *14*, 3107.
[47] N. Lorenzin, A. Abanades, *Int. J. Hydrogen Energy* **2016**, *41*, 6990.
[48] D. C. Upham, V. Agarwal, A. Khechfe, Z. R. Snodgrass, M. J. Gordon, H. Metiu, E. W. McFarland, *Science* **2017**, *358*, 917.
[49] M. Plevan, T. Geißler, A. Abánades, K. Mehravaran, R. K. Rathnam, C. Rubbia, D. Salmieri, L. Stoppel, S. Stückrad, T. Wetzel, *Int. J. Hydrogen Energy* **2015**, *40*, 8020.
[50] N. A. Kaffes, in *Steam Reforming of Methane on a Nickel Catalyst Suspended in Molten Sodium Phosphates*, California Institute of Technology, Ann Arbor, MI **1982**.
[51] A. Abánades, E. Ruiz, E. M. Ferruelo, F. Hernández, A. Cabanillas, J. M. Martínez-Val, J. A. Rubio, C. López, R. Gavela, G. Barrera, *Int. J. Hydrogen Energy* **2011**, *36*, 12877.
[52] T. Geißler, M. Plevan, A. Abánades, A. Heinzel, K. Mehravaran, R. K. Rathnam, C. Rubbia, D. Salmieri, L. Stoppel, S. Stückrad, A. Weisenburger, H. Wenninger, Th Wetzel, *Int. J. Hydrogen Energy* **2015**, *40*, 14134.
[53] A. Abánades, R. K. Rathnam, T. Geißler, A. Heinzel, K. Mehravaran, G. Müller, M. Plevan, C. Rubbia, D. Salmieri, L. Stoppel, *Int. J. Hydrogen Energy* **2016**, *41*, 8159.
[54] T.-G. Wi, Y.-J. Park, U. Lee, Y.-B. Kang, *Chem. Eng. J.* PA **2023**, *460*, 141558.
[55] C. Palmer, M. Tarazkar, H. H. Kristoffersen, J. Gelinas, M. J. Gordon, E. W. McFarland, H. Metiu, *ACS Catal.* **2019**, *9*, 8337.
[56] C. M. Hofberger, B. Dietrich, I. Durán Vera, R. Krumholz, L. Stoppel, N. Uhlenbruck, T. Wetzel, *Hydrogen* **2023**, *4*, 295.
[57] C. M. Hofberger, B. Dietrich, I. Durán Vera, R. Krumholz, L. Stoppel, N. Uhlenbruck, T. Wetzel, *Hydrogen* **2023**, *4*, 357.
[58] T. Geißler, A. Abánades, A. Heinzel, K. Mehravaran, G. Müller, R. K. Rathnam, C. Rubbia, D. Salmieri, L. Stoppel, S. Stückrad, A. Weisenburger, H. Wenninger, T. Wetzel, *Chem. Eng. J.* **2016**, *299*, 192.
[59] T. G. Geißler, in *Methanpyrolyse in einem Flüssigmetall-Blasensäulenreaktor*, Verlag Dr. Hut, Munich, Germany **2017**.
[60] E. A. Raiskaya, O. I. Krivonos, A. V. Babenko, O. B. Belskaya, *J. Anal. Appl. Pyrolysis* **2021**, *159*, 105328.
[61] S. S. Nagaraja, A. B. Sahu, S. Panigrahy, H. J. Curran, *Combust. Flame* **2021**, *233*, 111579.
[62] Y. V. Gavrilov, A. Y. Naletov, E. N. Mikhailova, G. S. Savin, *Coke Chem.* **2023**, *66*, 362.
[63] R. Clift, J. R. Grace, M. E. Weber, in *Bubbles, Drops, Particles*, Dover publications, inc. Mineaola, NY **2005**, p. 04864458.
[64] B. N. Thorat, A. V. Kulkarni, J. B. Joshi, *Chem. Eng. Technol.* **2001**, *24*, 815.
[65] Y. Zhang, Y. Cai, S. Hwang, G. Wilk, F. DeAngelis, A. Henry, K. H. Sandhage, *Sol. Energy* **2018**, *164*, 47.

© 2024 The Author(s). Energy Technology published by Wiley-VCH GmbH

21944296, 0, Downloaded from https://onlinelibrary.wiley.com/doi/10.1002/ente.202400183 by Christoph Hofberger , Wiley Online Library on [16/07/2024]. See the Terms and Conditions (https://onlinelibrary.wiley.com/terms-and-conditions) on Wiley Online Library for rules of use; OA articles are governed by the applicable Creative Commons License

[66] M. Kondo, M. Ishii, T. Muroga, *Fusion Eng. Des.* **2015**, *98–99*, 2003.
[67] M. Kondo, M. Tada, Y. Ohtsuka, Y. Hishinuma, T. Muroga, *Fusion Eng. Des.* **2019**, *146*, 2450.
[68] Z. Ye, X. Ma, P. He, Z. Wang, Q. Liu, Q. Yan, J. Wei, K. Zhang, F. Gou, *Nucl. Mater. Energy* **2019**, *20*, 100694.
[69] T. Haas, C. Schubert, M. Eickhoff, H. Pfeifer, *Metals* **2021**, *11*, 664.
[70] T. Loimer, G. Machu, U. Schaflinger, *Chem. Eng. Sci.* **2004**, *59*, 809.
[71] F. M. Al-Oufi, I. W. Cumming, C. D. Rielly, *Can. J. Chem. Eng.* **2010**, *88*, 482.
[72] N. Uhlenbruck, B. Dietrich, C. Hofberger, L. Stoppel, T. Wetzel, *Energy Tech* **2022**, *10*, 2200654.
[73] A. A. Kulkarni, J. B. Joshi, *Ind. Eng. Chem. Res.* **2005**, *44*, 5873.
[74] A. Capponi, E. W. Llewellin, *Int. J. Multiphase Flow* **2019**, *114*, 66.
[75] A. Agudelo, C. Cortés, *Energy* **2010**, *35*, 679.
[76] E. Camarasa, C. Vial, S. Poncin, G. Wild, N. Midoux, J. Bouillard, *Chem. Eng. Process.* **1999**, *38*, 329.
[77] M. Sano, K. Mori, *Trans. Jpn. Inst. Met.* **1976**, *17*, 344.
[78] G. A. Irons, R. I. Guthrie, *Metall. Trans. B* **1978**, *9*, 101.
[79] W. L. Peng, G. Yang, L.-S. Fan, *Ind. Eng. Chem. Res.* **2002**, *41*, 1666.
[80] H. Mirsandi, M. W. Baltussen, E. A. J. F. Peters, D. E. A. van Odyck, J. van Oord, D. van der Plas, J. A. M. Kuipers, *Int. J. Multiphase Flow* **2020**, *131*, 103363.
[81] G. Q. Yang, B. Du, L. S. Fan, *Chem. Eng. Sci.* **2007**, *62*, 2.
[82] H. N. Oguzrea, A. Prosperetti, *J. Fluid Mech.* **1993**, *257*, 111.
[83] M. T. Dhotre, J. B. Joshi, *Chem. Eng. J.* **2007**, *125*, 149.
[84] T. Miyahara, M. Iwata, T. Takahashi, *J. Chem. Eng. Japan* **1984**, *17*, 592.
[85] W. Zhang, R. B. Tan, *Chem. Eng. Sci.* **2000**, *55*, 6243.
[86] H. Ogihara, H. Tajima, H. Kurokawa, *React. Chem. Eng.* **2020**, *5*, 145.
[87] M. Nitsche, in *Kolonnen-Fibel: Für die Praxis im chemischen Anlagenbau*, Springer, Verlag, Heidelberg **2015**.
[88] Y. Kato, T. Nozaki, K. Nakanishi, T. Fuii, T. Emi, *Tetsu-to-Hagané* **1984**, *70*, 380.
[89] D. J. McCann, R. G. H. Prince, *Chem. Eng. Sci.* **1969**, *24*, 801.
[90] M. I. Hossain, Q. X. Pang, S. Q. Pang, Y. Yang, R. Lau, *Ind. Eng. Chem. Res.* **2011**, *50*, 389.
[91] E. S. Gaddis, A. Vogelpohl, *Chem. Eng. Sci.* **1986**, *41*, 97.
[92] L. Kirkup, R. B. Frenkel, in *An introduction to Uncertainty in Measurement: Using the GUM (guide to the Expression of Uncertainty in Measurement)*, Cambridge University Press, Cambridge, UK **2006**.
[93] N. Rahimi, D. Kang, J. Gelinas, A. Menon, M. J. Gordon, H. Metiu, E. W. McFarland, *Carbon* **2019**, *151*, 181.
[94] B. J. L. Pérez, J. A. M. Jiménez, R. Bhardwaj, E. Goetheer, M. van Sint Annaland, F. Gallucci, *Int. J. Hydrogen Energy* **2021**, *46*, 4917.
[95] N. Zaghloul, S. Kodama, H. Sekiguchi, *Chem. Eng. Technol.* **2021**, *44*, 1986.
[96] J. Kim, C. Oh, H. Oh, Y. Lee, H. Seo, Y. K. Kim, *Carbon* **2023**, *207*, 449.
[97] Y. Zhang, J. R. G. Evans, S. Yang, *J. Chem. Eng. Data* **2011**, *56*, 328.
[98] A. F. Holleman *Lehrbuch der anorganischen Chemie*, 91st ed., De Gruyter, Berlin **1985**.
[99] H. Preston-Thomas *Metrologia* **1990**, *27*, 3.

© 2024 The Author(s). Energy Technology published by Wiley-VCH GmbH

21944296, 0, Downloaded from https://onlinelibrary.wiley.com/doi/10.1002/ente.202400183 by Christoph Hofberger , Wiley Online Library on [16/07/2024]. See the Terms and Conditions (https://onlinelibrary.wiley.com/terms-and-conditions) on Wiley Online Library for rules of use; OA articles are governed by the applicable Creative Commons License